

5-2018

Electromagnetic Compatibility Research in Wire Harnesses and CAN Transceivers

Jongtae Ahn

Clemson University, jongtaa@clemson.edu

Follow this and additional works at: https://tigerprints.clemson.edu/all_dissertations

Recommended Citation

Ahn, Jongtae, "Electromagnetic Compatibility Research in Wire Harnesses and CAN Transceivers" (2018). *All Dissertations*. 2165.
https://tigerprints.clemson.edu/all_dissertations/2165

This Dissertation is brought to you for free and open access by the Dissertations at TigerPrints. It has been accepted for inclusion in All Dissertations by an authorized administrator of TigerPrints. For more information, please contact kokeefe@clemson.edu.

ELECTROMAGNETIC COMPATIBILITY RESEARCH IN WIRE HARNESSSES
AND CAN TRANSCEIVERS

A Dissertation
Presented to
the Graduate School of
Clemson University

In Partial Fulfillment
of the Requirements for the Degree
Doctor of Philosophy
Electrical Engineering

by
Jongtae Ahn
May 2018

Accepted by:
Pingshan Wang, Committee Chair
Todd Hubing
Adam Hoover
Anthony Q. Martin
Jeong-Rock Yoon

ABSTRACT

This dissertation develops methods how to design wire harnesses reducing common mode components and to analyze the conversion from differential mode to common mode. The three chapters presented are design methods how to figure out the impact of the common-mode components, not only describe the test results but provide important insight as to how the design related to radiated emissions.

In the first chapter of this dissertation, the method designing wire harnesses has been presented to match the electrical balance of the circuit board (PCB). This is accomplished via calculating the current division factor (CDF) of the wire harnesses and the PCB, which provides us with the electrical balance of a transmission line. To reduce the amount of common-mode currents induced on the harness, matching the imbalance of the wire harness to the imbalance of its source and termination is essential.

The second chapter explores Controller Area Network (CAN) characteristics. Unintentional common-mode components of the CAN transceivers are analyzed and evaluated to determine how much common-mode voltage they produce in various circumstances.

The final chapter provide valuable understanding such that ground proximity impacts on the common-mode currents of wire harnesses. The electrical balance change of the wire harness depending on the distance from ground structures is highlighted. It is also analyzed that losing the ground wire impacts on the common-mode excitation.

DEDICATION

This dissertation is dedicated to my family and Kyungshin who support me unconditionally, but especially my wife and daughters.

ACKNOWLEDGMENTS

First of all, I would like to give my best words of gratitude to Dr. Todd Hubing for serving as my advisor on this dissertation. This dissertation could not have been completed without his passionate guidance. With Dr. Hubing, I learned about the field of electromagnetic compatibility thoroughly. Being his student was a privilege that I would never forget.

I would be also like to thank the other committee members: Drs. Pingshan Wang, Adam Hoover, Anthony Q. Martin, and Jeong-Rock Yoon. I appreciate your support and guidance.

Lastly, I would like to thank my wife for her patience and support. I could be going further because of all loves from her.

TABLE OF CONTENTS

	Page
TITLE PAGE	i
ABSTRACT	ii
DEDICATION	iii
ACKNOWLEDGMENTS	iv
LIST OF TABLES	vii
LIST OF FIGURES	viii

CHAPTER

I.	APPLICATION OF IMBALANCE DIFFERENCE METHOD TO THE EMC DESIGN OF AUTOMOTIVE WIRE HARNESSSES	1
	Abstract	1
	1.1 Introduction	1
	1.2 Current Division Factor Calculation	3
	1.3 The Wire Harness Design for Twisted Pair and Ground Wires.....	11
	1.4 Measurement Results	14
	1.5 Conclusion	17
	References	17
II.	EVALUATION OF THE COMMON MODE VOLTAGE GENERATED BY DIFFERENT CAN TRANSCEIVERS	19
	Abstract	19
	2.1 Introduction	19
	2.2 Test Setup for Measuring CM Voltages by CAN Drivers	20
	2.3 Experiment Results	23
	2.4 Conclusion	30
	References	30

Table of Contents (Continued)

Page

III.EFFECT OF GROUND PROXIMITY ON COMMON-MODE CURRENT IN WIRE HARNESSSES.....	32
Abstract	32
3.1 Introduction.....	32
3.2 Wire Harness Geometry under Study	34
3.3 Results and Discussion.....	38
3.4 Conclusion	46
References	47

LIST OF TABLES

Table		Page
1.1	Number of variables needed to solve a system with N conductors.....	4
1.2	Circuit board and wire harness parameters that affect the CDF	14
2.1	Measured transition times and CM voltages peaks and CM current peaks .	27

LIST OF FIGURES

Figure	Page
1.1	Validation of ATLC2 capacitance calculation.....5
1.2	Ribbon cable consisting of 4 wires6
1.3	Capacitance calculation results using ATLC28
1.4	Capacitance calculation matrix with the simulation results.....9
1.5	PCB board traces over a return plane..... 10
1.6	PCB configuration and corresponding current division factors..... 11
1.7	Wire bundle configurations and corresponding current division factors 12
1.8	CDF's of four-wire bundle compared to the PCB configuration..... 12
1.9	The other types with five-wire bundles compared to the PCB configuration 13
1.10	Test set-up and cross section of wire harnesses 14
1.11	The results of antenna mode currents in two wire harnesses 16
2.1	Schematic view of CAN transceiver test set-up.....20
2.2	The fabricated printed circuit board top view22
2.3	Test set-up and probe connection configuration22
2.4	Measured differential signal voltage and CM voltage for the five transceivers23
2.5	Slew rates and time offset in the transition25
2.6	CM currents measurements for the five transceivers.....26
2.7	CM voltages and currents at different baud rates.....28
2.8	Frequency domain representation of the CM voltage and currents29

LIST OF FIGURES (Continued)

Figure	Page
3.1 Wire harnesses in an automobile.....	33
3.2 Schematic view of the test environment and wire harness geometry	36
3.3 Test setup for each bending configuration	37
3.4 Common-mode excitation on the vertical bended wire harness	39
3.5 The quarter-wave monopole antenna modelling.....	40
3.6 Full-wave simulation configuration	41
3.7 FEKO results for the antenna-mode currents at the lower voltage source...41	
3.8 Comparison of the common-mode currents with the vertical bending and with the parallel bending to the copper plane	43
3.9 Test set-up for the detached twin wire pair from the ground wire.....	44
3.10 Effect of losing the ground wire from the signal wires.....	46

CHAPTER ONE

APPLICATION OF IMBALANCE DIFFERENCE METHOD TO THE EMC DESIGN OF AUTOMOTIVE WIRE HARNESSSES

Abstract

Common mode currents induced on wiring harnesses often play a key role in the electromagnetic compatibility of automotive components and systems. Designing the electrical balance of the harness to match the electrical balance of the circuit board prevents mode conversion from taking place at the board-cable interface. This paper describes how wire harnesses can be designed to have imbalance factors that match typical circuit board geometries.

1.1 Introduction

Unwanted radiated emissions can present significant challenges to the designers of automotive electronics. A primary source of these radiated emissions is the common-mode (or antenna-mode) current induced on the wire harnesses. Even small cars today can have a thousand meters of wire harnesses, and luxury cars may have four times more than that [1]. Wire harness emissions can cause disturbances to numerous HF devices (e.g. FM radio, Bluetooth, GPS and GSM devices) [2]. However, shielded wires or coaxial cables are rarely used in automotive environments due to cost, weight, flexibility and bonding issues. It is important therefore, to address the issue of unintended radiated emissions from wire harnesses without shielding whenever possible.

At the frequencies where radiated emissions are measured, the signals in a wiring harness are propagated as differential-mode currents, while the radiated emissions primarily result from the common-mode currents. The generation of CM currents from

differential-mode (DM) signals has been studied extensively. A very powerful method for modeling differential-mode to common-mode conversion was introduced in [3, 4]. This approach is commonly referred to as the Imbalance Difference Theory (IDT). IDT defines the concept of electrical balance in a transmission line (TL) and an imbalance factor (or current division factor) that precisely quantifies this balance [5, 6]. IDT demonstrates that changes in the electrical balance on TLs results in a conversion between DM propagation and CM propagation. The amplitude of the induced voltage driving the CM propagation can be accurately expressed as the product of the DM voltage and the change in the imbalance factor at any given point along a transmission line. IDT provides great insight into the DM-to-CM conversion mechanism and provides an easy way of modeling this conversion in many practical situations.

In [7], a method for computing the per-unit-length generalized capacitance matrix in a multi-conductor transmission line such as a wire harness was presented. This capacitance matrix can be used to calculate the imbalance factor associated with any given signal propagation mode.

This paper explores the possibility of designing wire harnesses that mimic the imbalance factors that the signals experience as they propagate along circuit board traces. This approach prevents differential-mode signals that propagate from a circuit board to a wiring harness from generating common-mode currents on the harness. Section 1.2 explains the calculation of the capacitances in a multi-conductor system using 2D field solvers, then derives the current division factor based on these capacitances. Section 1.3 compares the calculated current division factors for various wire bundle cross-sections and

discusses the effect of various parameters on the calculation results. Section 1.4 validates the concept presented in the paper using experimental results. Finally, the discussion is summarized in Section 1.5.

1.2 Current Division Factor Calculation

In a wire harness with N wires, we can define a self-capacitance for each wire and a mutual capacitance between each wire pair. The self- and mutual-capacitances per unit length of each wire can be calculated using a 2D electric field solver. For the calculations in this paper, we used a free solver called ATLC2. ATLC2 does not solve for the self- and mutual-capacitances directly, but it can calculate the total capacitance between any two sets of conductors. The generalized capacitance matrix can be expressed as below.

$$\begin{bmatrix} Q_1 \\ Q_2 \\ \cdot \\ \cdot \\ Q_n \end{bmatrix} = \begin{bmatrix} c_{11} & c_{12} & \cdots & c_{1n} \\ c_{21} & c_{22} & \cdots & c_{2n} \\ \cdots & \cdots & \cdots & \cdots \\ c_{n1} & c_{n2} & \cdots & c_{nn} \end{bmatrix} \begin{bmatrix} V_1 \\ V_2 \\ \cdot \\ \cdot \\ V_n \end{bmatrix} \quad (1.1)$$

Coefficients of the form c_{ii} represent the self-capacitance of the i^{th} conductor. Coefficients of the form c_{ij} where $i \neq j$ are referred to as coefficients of induction. These coefficients satisfy the relation $c_{ij}=c_{ji}$. The relation between these coefficients and the mutual capacitance between the i^{th} and j^{th} conductor is $C_{ij}=-c_{ij}$. Let's define the mutual capacitance as c_{ij} rather than use C_{ij} . For a harness with N wires, there are N^2 matrix elements, however since $c_{ij}=c_{ji}$, the number of independent variables is $N(N+1)/2$. The number of variables needed to solve a system with N conductors are shown in Table 1.1.

Table 1.1. Number of variables needed to solve a system with N conductors

N	Number of variables
2	3
3	6
4	10
5	15

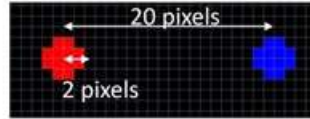
To calculate the mutual and self-capacitances using a 2D capacitance solver, a non-zero voltage is assigned to one wire while the other wires are held to zero potential (ground). The 2D solver calculates the charge density induced on the wire with non-zero voltage and uses that to obtain its capacitance per unit length. For example, if the non-zero voltage is applied only to Wire 1, the capacitance per unit length obtained using a 2D solver represents the capacitance per unit length of Wire 1 to all other wires and infinity, which is $C_1 = c_{11} + c_{12} + c_{13} + \dots + c_{1n}$. Repeating this calculation for the remaining wires yields N equations in a harness with N wires. Secondly, if the same non-zero voltage is applied to Wire 1 and Wire 2 while the remaining wires are grounded, the calculated capacitance represents the quantity $C_{total} = c_{11} + c_{13} + c_{14} \dots + c_{1n} + c_{22} + c_{23} + \dots + c_{2n}$. Note that mutual capacitance c_{12} vanished because conductor 1 and 2 is regarded as connected which means same potential between the two conductors. Likewise, repeating this calculation for the remaining wires yields by putting non-zero voltage to two conductors among N conductors is $N C_2 = \frac{N \cdot (N-1)}{2}$ equations. Therefore, total number of the equations is

$$N + \frac{N \cdot (N-1)}{2} = \frac{N(N+1)}{2}$$

which equals the number of variables. To reduce numerical

error associated with these calculations, redundant equations are added in order to create

an over-determined system. Additional equations that three conductors are the positive non-zero voltage are used to make the system to be over-determined.



d:5mm, a=0.5mm, ratio(d/2a)=10

Distance(cm)	Diameter(mm)	Capacitance			ratio(d/2a)
		ATLC2(pF)	Calculated values(pF/m)	Variance(pF)	
0.3	0.64	12.68	12.49	0.19	4.69
0.4	0.64	11.25	11.04	0.21	6.25
0.5	0.64	10.34	10.13	0.21	7.81
10	10	9.44	9.29	0.15	10.00
15	10	8.29	8.18	0.11	15.00
1	0.64	8.21	8.08	0.13	15.63
2	0.64	6.80	6.73	0.07	31.25
15	4	6.51	6.44	0.07	37.50
3	0.64	6.19	6.13	0.06	46.88
15	3	6.10	6.04	0.06	50.00
4	0.64	5.81	5.76	0.05	62.50
15	2	5.59	5.55	0.04	75.00
15	1	4.88	4.88	0.00	150.00
10	0.64	4.84	4.84	0.00	156.25
20	1	4.62	4.64	0.02	200.00
15	0.64	4.48	4.52	0.04	234.38
30	1	4.26	4.35	0.09	300.00
60	2	4.26	4.35	0.09	300.00
50	1	3.77	4.03	0.26	500.00
70	1	3.24	3.84	0.60	700.00

Fig. 1.1. Validation of ATLC2 capacitance calculation

Fig. 1.1 shows ATLC2 calculations for the capacitance of a twin-wire pair using ATLC2 and an analytical calculation. ATLC2 uses screen pixels to define the cross-section geometry. For these calculations, the number of conductor pixels is twelve. One pixel represents a square that is 0.25 mm on a side. The mutual capacitance between the wires can be calculated analytically as,

$$C = \frac{\pi\epsilon}{\cosh^{-1}(d/2a)} \quad (1.2)$$

The ‘d’ represents center-to-center distance between the conductors and the ‘a’ represents the conductor radius. The results in Fig. 1.1 indicate that ATLC2 calculates a capacitance within 2% of the analytical value. In ATLC2, the voltage on the wire is represented by the color. The red color represents a positive voltage, blue is negative, and green is ground or zero potential. The general process to calculate the self-capacitance using ATLC2 is:

- 1) Define the geometry of the test environment.
- 2) Draw the conductors and any dielectric insulators.
- 3) Assign a positive voltage or a zero potential to each conductor.
- 4) Run the program to calculate the total capacitance.
- 5) Repeat this process with different voltage assignments until you have enough data to build a capacitance matrix to derive self-capacitance of each conductor.

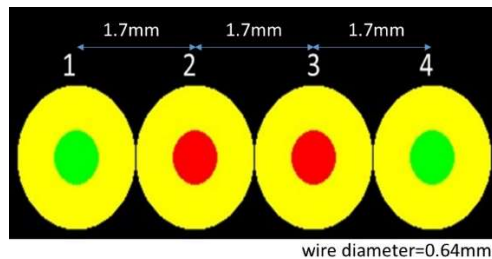


Fig. 1.2. Ribbon cable consisting of 4 wires

Fig. 1.2 shows a ribbon cable that has 4 wires with a polystyrene insulator ($\epsilon_r=2.5$). The inner two wires have a positive voltage represented by their red color. The outer two (green) wires represent the conductors used for return current. Note that in this configuration (and the remaining configurations to be examined in this paper) the “differential mode” currents flow in the same direction on a pair of conductors and return on other conductors (normally labeled “ground”). This represents currents that are

normally labeled as the common-mode components of a differential signal, but do not result in significant radiated emissions because they return on a nearby “ground” conductor. The common-mode currents that we are concerned with in this paper are the currents induced that flow in the same direction on all of the conductors. These currents are sometimes referred to as “antenna mode” currents [5].

The current division factor (CDF) for the configuration in Fig. 3 can be calculated using the self-capacitance terms (i.e. capacitances to infinity) as below,

$$CDF = \frac{c_{22} + c_{33}}{c_{11} + c_{22} + c_{33} + c_{44}} \quad (1.3)$$

For calculating the self and mutual capacitances using ATLC2, we need at least 10 equations to complete the capacitance matrix.















Geometry and Charges	Results
	Conductor 1 only $c_{11} + c_{12} + c_{13} + c_{14} = 34.237$ (1)
	Conductor 2 only $c_{12} + c_{22} + c_{23} + c_{24} = 52.459$ (2)
	Conductor 3 only $c_{13} + c_{23} + c_{33} + c_{34} = 52.460$ (3)
	Conductor 4 only $c_{14} + c_{24} + c_{34} + c_{44} = 34.238$ (4)
	Conductor 1&2 $(c_{11} + c_{22}) + c_{13} + c_{14} + c_{23} + c_{24} = 37.016$ (5)
	Conductor 1,2,&3 $(c_{11} + c_{22} + c_{33}) + c_{14} + c_{24} + c_{34} = 36.684$ (6)
	Conductor 1&3 $(c_{11} + c_{33}) + c_{12} + c_{23} + c_{14} + c_{34} = 79.628$ (7)
	Conductor 1&4 $(c_{11} + c_{44}) + c_{12} + c_{13} + c_{34} + c_{24} = 61.945$ (8)
	Conductor 2&4 $(c_{22} + c_{44}) + c_{12} + c_{23} + c_{14} + c_{34} = 79.629$ (9)
	Conductor 2,3,&4 $(c_{22} + c_{33} + c_{44}) + c_{12} + c_{13} + c_{14} = 36.686$ (10)
	Conductor 2&3 $(c_{22} + c_{33}) + c_{12} + c_{13} + c_{24} + c_{24} = 58.895$ (11)
	Conductor 3&4 $(c_{33} + c_{44}) + c_{13} + c_{23} + c_{14} + c_{24} = 37.018$ (12)
	Conductor 1,3,&4 $(c_{11} + c_{33} + c_{44}) + c_{12} + c_{23} + c_{24} = 57.608$ (13)
	Conductor 1,2,&4 $(c_{11} + c_{22} + c_{44}) + c_{13} + c_{23} + c_{34} = 57.607$ (14)

Fig. 1.3. Capacitance calculation results using ATLC2

Fig. 1.3 shows the calculated capacitances between various sets of conductors. $N=4$, so there are $4(4+1)/2=10$ independent coefficients to be determined. Four redundant simulations were performed to reduce the simulation error.

$$\begin{array}{l}
(1) \\
(2) \\
(3) \\
(4) \\
(5) \\
(6) \\
(7) \\
(8) \\
(9) \\
(10) \\
(11) \\
(12) \\
(13) \\
(14)
\end{array}
\begin{bmatrix}
34.237 \\
52.459 \\
52.460 \\
34.238 \\
37.016 \\
36.684 \\
79.628 \\
61.945 \\
79.629 \\
36.686 \\
58.895 \\
37.018 \\
57.608 \\
57.607
\end{bmatrix}
=
\begin{bmatrix}
1 & 1 & 1 & 1 & 0 & 0 & 0 & 0 & 0 & 0 \\
1 & 0 & 0 & 0 & 1 & 0 & 0 & 1 & 1 & 0 \\
0 & 0 & 1 & 0 & 0 & 1 & 0 & 1 & 1 & 0 \\
0 & 0 & 0 & 1 & 0 & 0 & 1 & 0 & 1 & 1 \\
1 & 0 & 1 & 1 & 1 & 1 & 1 & 0 & 0 & 0 \\
1 & 0 & 0 & 1 & 1 & 0 & 1 & 1 & 1 & 1 \\
1 & 1 & 0 & 1 & 0 & 1 & 0 & 1 & 1 & 0 \\
1 & 1 & 1 & 0 & 0 & 0 & 1 & 0 & 1 & 1 \\
0 & 1 & 0 & 1 & 1 & 1 & 0 & 0 & 1 & 1 \\
0 & 1 & 1 & 1 & 1 & 1 & 0 & 1 & 0 & 1 \\
0 & 1 & 1 & 0 & 1 & 0 & 1 & 1 & 1 & 0 \\
0 & 0 & 1 & 1 & 0 & 1 & 1 & 1 & 0 & 1 \\
1 & 1 & 0 & 0 & 0 & 1 & 1 & 1 & 0 & 1 \\
1 & 0 & 1 & 0 & 1 & 1 & 0 & 0 & 1 & 1
\end{bmatrix}
\begin{bmatrix}
c_{11} \\
c_{12} \\
c_{13} \\
c_{14} \\
c_{22} \\
c_{23} \\
c_{24} \\
c_{33} \\
c_{34} \\
c_{44}
\end{bmatrix}
=
\begin{bmatrix}
c_{11} \\
c_{12} \\
c_{13} \\
c_{14} \\
c_{22} \\
c_{23} \\
c_{24} \\
c_{33} \\
c_{34} \\
c_{44}
\end{bmatrix}
=
\begin{bmatrix}
1 & 1 & 1 & 1 & 0 & 0 & 0 & 0 & 0 & 0 \\
1 & 0 & 0 & 0 & 1 & 0 & 0 & 1 & 1 & 0 \\
0 & 0 & 1 & 0 & 0 & 1 & 0 & 1 & 1 & 0 \\
0 & 0 & 0 & 1 & 0 & 0 & 1 & 0 & 1 & 1 \\
1 & 0 & 1 & 1 & 1 & 1 & 1 & 0 & 0 & 0 \\
1 & 0 & 0 & 1 & 1 & 0 & 1 & 1 & 1 & 1 \\
1 & 1 & 0 & 1 & 0 & 1 & 0 & 1 & 1 & 0 \\
1 & 1 & 1 & 0 & 0 & 0 & 1 & 0 & 1 & 1 \\
0 & 1 & 0 & 1 & 1 & 1 & 0 & 0 & 1 & 1 \\
0 & 1 & 1 & 1 & 1 & 1 & 0 & 1 & 0 & 1 \\
0 & 1 & 1 & 0 & 1 & 0 & 1 & 1 & 1 & 0 \\
0 & 0 & 1 & 1 & 0 & 1 & 1 & 1 & 0 & 1 \\
1 & 1 & 0 & 0 & 0 & 1 & 1 & 1 & 0 & 1 \\
1 & 0 & 1 & 0 & 1 & 1 & 0 & 0 & 1 & 1
\end{bmatrix}^{-1}
\begin{bmatrix}
34.237 \\
52.459 \\
52.460 \\
34.238 \\
37.016 \\
36.684 \\
79.628 \\
61.945 \\
79.629 \\
36.686 \\
58.895 \\
37.018 \\
57.608 \\
57.607
\end{bmatrix}$$

Fig. 1.4. Capacitance calculation matrix with the simulation results

Fig. 1.4 shows the capacitance matrix obtained from the simulation results. We have 14 equations and 10 variables so that the matrix is not rectangular. MATLAB was used to solve the over-determined system using the ‘mldivide’ (‘\’) function, which provides a least-squares solution minimizing the length of the vector $AX - B$. The calculated self-capacitances in this example are,

$$c_{11} = 2.749, c_{22} = 1.224, c_{33} = 1.224, c_{44} = 2.749 \quad (1.4)$$

and the current division factor (CDF) is,

$$CDF = \frac{c_{22} + c_{33}}{c_{11} + c_{22} + c_{33} + c_{44}} = 0.3081 \quad (1.5)$$

If the wire insulation is changed to Teflon ($\epsilon_r=2.02$), the calculated self-capacitance of each wire and the current division factor become,

$$c_{11} = 2.6039, c_{22} = 1.2053, c_{33} = 1.2058, c_{44} = 2.6049 \quad (1.6)$$

and,

$$CDF = \frac{c_{22} + c_{33}}{c_{11} + c_{22} + c_{33} + c_{44}} = 0.3164 \quad (1.7)$$

The transmission line is more balanced when the relative permittivity of the insulation is lower. Higher permittivity dielectrics capture more of the electric field from the outer conductors making their self-capacitances closer to the self-capacitances of the inner conductors.

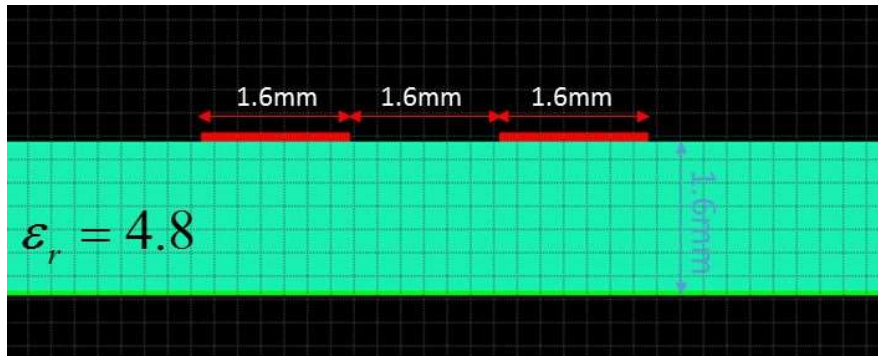


Fig. 1.5. PCB board traces over a return plane

Fig. 1.5 shows an example of a printed circuit board (PCB) board cross section. In this example current flows out on a pair of traces and returns on a solid plane 1.6 mm below the traces. The traces are separated by 1.6 mm. The trace width is 1.6 mm and the insulation material is FR4 ($\epsilon_r=4.8$). The traces are conductors 1 and 2. The return plane is conductor 3. The calculated self-capacitances and current division factor are,

$$c_{11}=0.2940, c_{22}=0.2940, c_{33}=7.1220 \quad (1.8)$$

and

$$CDF = \frac{c_{11} + c_{22}}{c_{11} + c_{22} + c_{33}} = 0.0763 \quad (1.9)$$

If the return plane is moved farther from traces, the current division factor increases, which means the circuit is more balanced. For example, the calculated current division factor increases to 0.0844 when the return plane is 2.6 mm away from traces.

1.3 The Wire Harness Design for Twisted Pair and Ground Wires

Based on the calculation of the self-capacitances in a multi-conductor wire harness, the current division factor can be optimized to match the current division factor of the components on each end to eliminate differential-mode to common-mode current conversion.

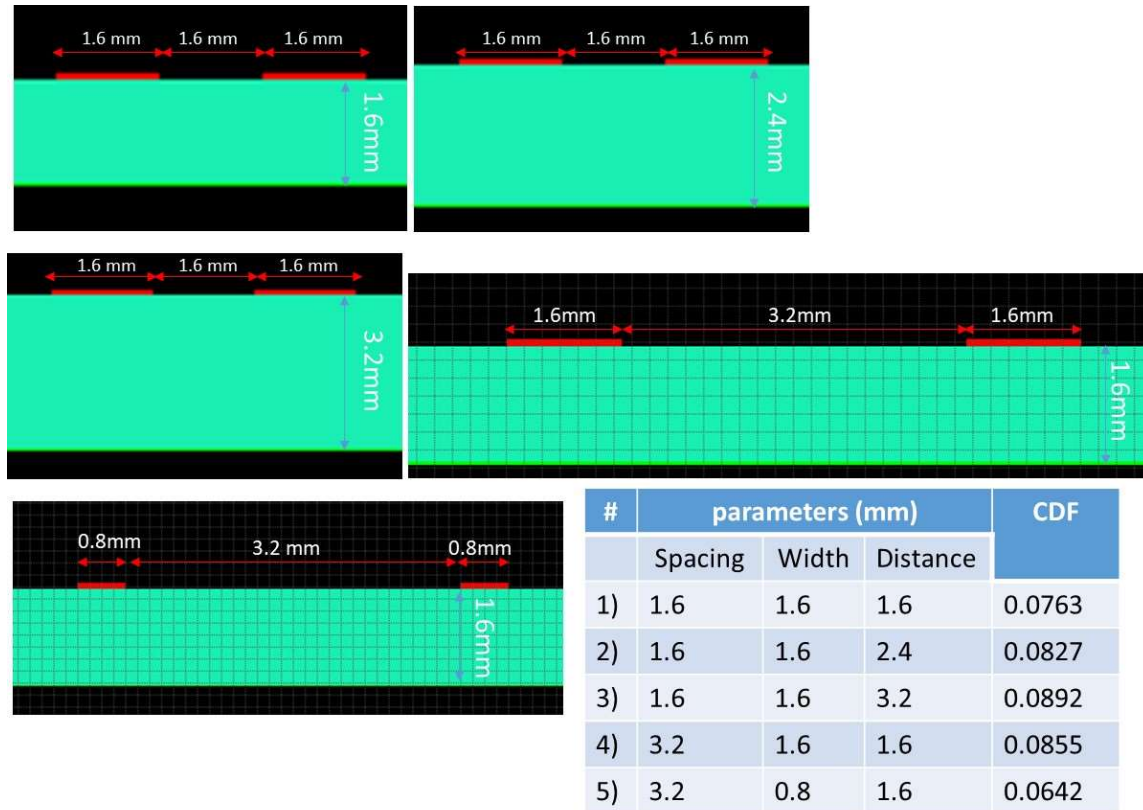


Fig. 1.6. PCB configurations and corresponding current division factors

Fig. 1.6 shows the current division factors calculated for several PCB geometries. All of the geometries are fairly unbalanced with CDFs ranging from 0.0642 to 0.0892. The

different configurations demonstrate that parameters of the PCB geometry can be adjusted to influence the current division factor. Structures with wider return planes are more unbalanced. (A theoretical circuit board with an infinitely wide return plane would be perfectly unbalanced with a CDF of 0.0) When the trace spacing is greater, the circuit is more balanced. When the trace width becomes smaller, the circuit becomes more unbalanced.

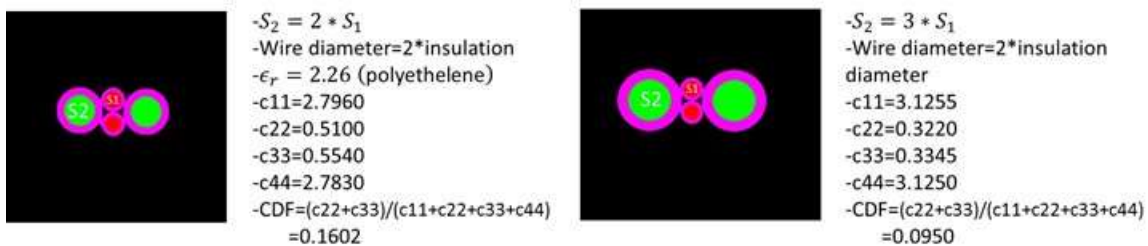


Fig. 1.7. Wire bundle configurations and corresponding current division factors

Fig. 1.7 shows two wire bundle configurations and their corresponding current division factors. The one on the right has a current division factor similar to that of typical PCB configuration. The cross-sectional area of the return path wires is greater than that of the signal wires. The diameter of the return wires is twice the insulation thickness. The return wires are located next to the signal wires to capture as much of the electric field from the signal wires as possible and reduce the CDF of the wire bundle.

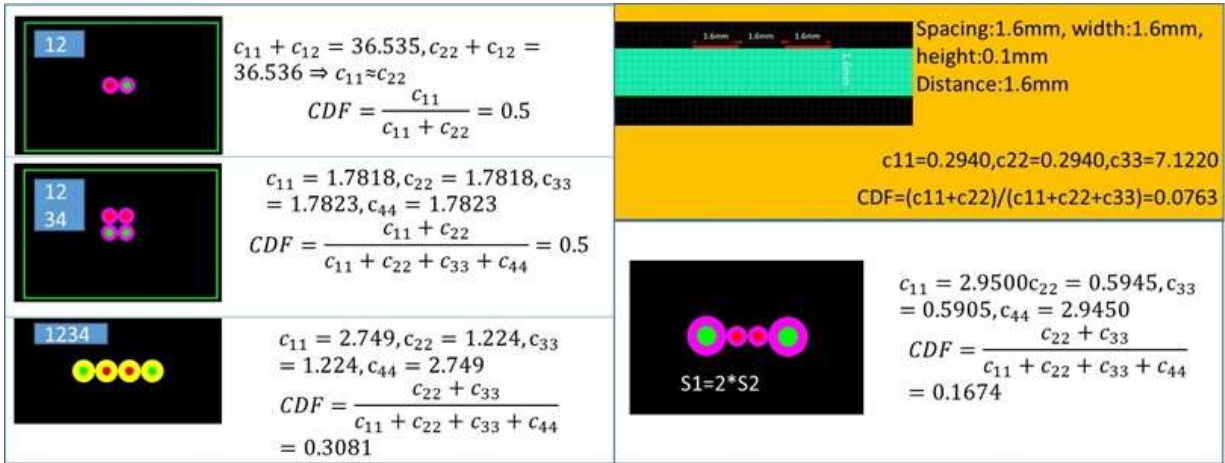


Fig. 1.8. CDFs of four-wire bundles compared to the PCB configuration

Fig. 1.8 shows the calculated current division factors for various wire harness geometries. As expected, the symmetric geometries are perfectly balanced (CDF = 0.5). The current division factor is reduced if the return wires are thicker than the signal wires. The ribbon cable is more unbalanced than the wire bundle even though the return wires are thicker due to the lack of close proximity between the signal and return conductors.

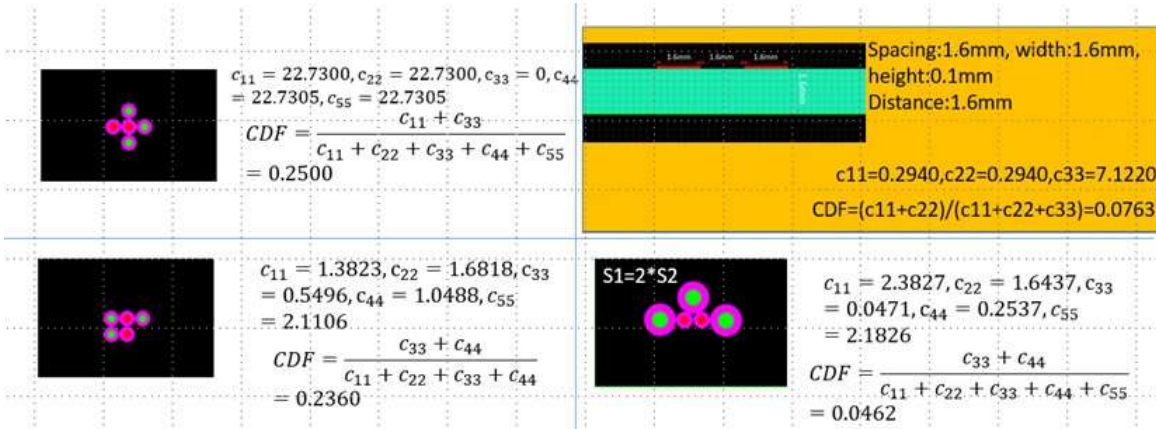


Fig. 1.9. The other types with five-wire bundles compared to the PCB configuration

Fig. 1.9 shows the calculated current division factors for various five wire bundles. These wire bundles are more unbalanced than the previous four wire bundles. Nevertheless, the imbalance of the wire harnesses is not enough to match the current division factor for

the PCB unless the case that the return wires are much thicker than signal wires. Circuit board and wire harness parameters that affect the CDF are listed in Table 1.2.

Table 1.2. Circuit board and wire harness parameters that affect the CDF

PCB board	Wire harness
Material of the substrate	Insulation material of wires
Separation width between traces	Wire geometry
Distance between traces and ground plane	Wire thickness
Trace width	Number of return conductors

1.4 Measurement Results

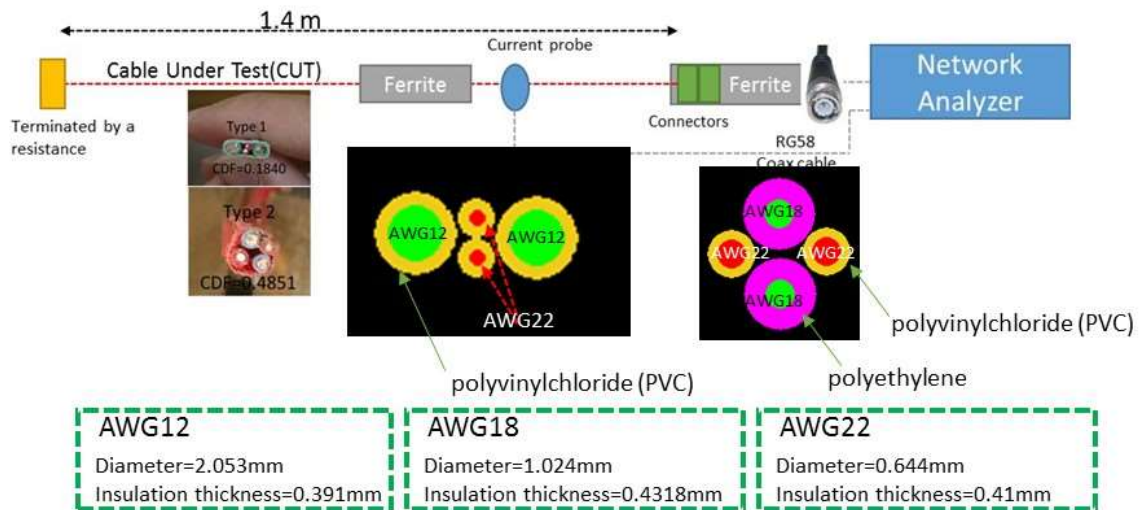


Fig. 1.10. Test set-up and cross sections of wire harnesses

Generally speaking, signals propagating on circuit board traces over a current return plane have very low CDFs (i.e. are very unbalanced). Therefore, to reduce the common-mode current induced on a wire harness attached to a circuit board, it is desirable for the harness to have a CDF that is as low as possible. To illustrate this, the test set-up in Fig. 1.10 was used to measure the common-mode current induced at the interface between a

coaxial cable (CDF = 0.0) and two different wire harnesses. The one on the left is made with AGW12 and AWG22 wires (CDF=0.1840). The one on the right is made with AWG18 and AWG22 (CDF=0.4851). The current division factors for the two harnesses were calculated using the method described in Section 1.2.

For this measurement, the network analyzer sends a signal through a coaxial cable (CDF=0.0) which connects to one the wire harness being evaluated. A current probe measures the common-mode current induced on the wire harness due to the changes in the imbalance that occurs at the coax-to-wire-harness interface. The wire harness termination is matched to the characteristic impedance of the harnesses being evaluated (68 ohms in both cases) and ferrites are places on the cables to dampen sharp resonances.

The change in the CDF at the interface between the coaxial cable and wire harness being evaluated equals the current division factor of the wire harness because the current division factor of the coaxial cable is zero. The harness with the lower CDF is expected to generate less common-mode current, because it is better matched to the coax. The difference in the common-mode current induced by the two harnesses should be equal to the difference in their CDFs. Expressed in decibels, this difference is,

$$\Delta h_1 = 0.1840, \Delta h_2 = 0.4851 \quad (1.10)$$

$$20 \log(\Delta h) = 20 \log\left(\frac{\Delta h_2}{\Delta h_1}\right) = 7.88 \text{ dB} \quad (1.11)$$

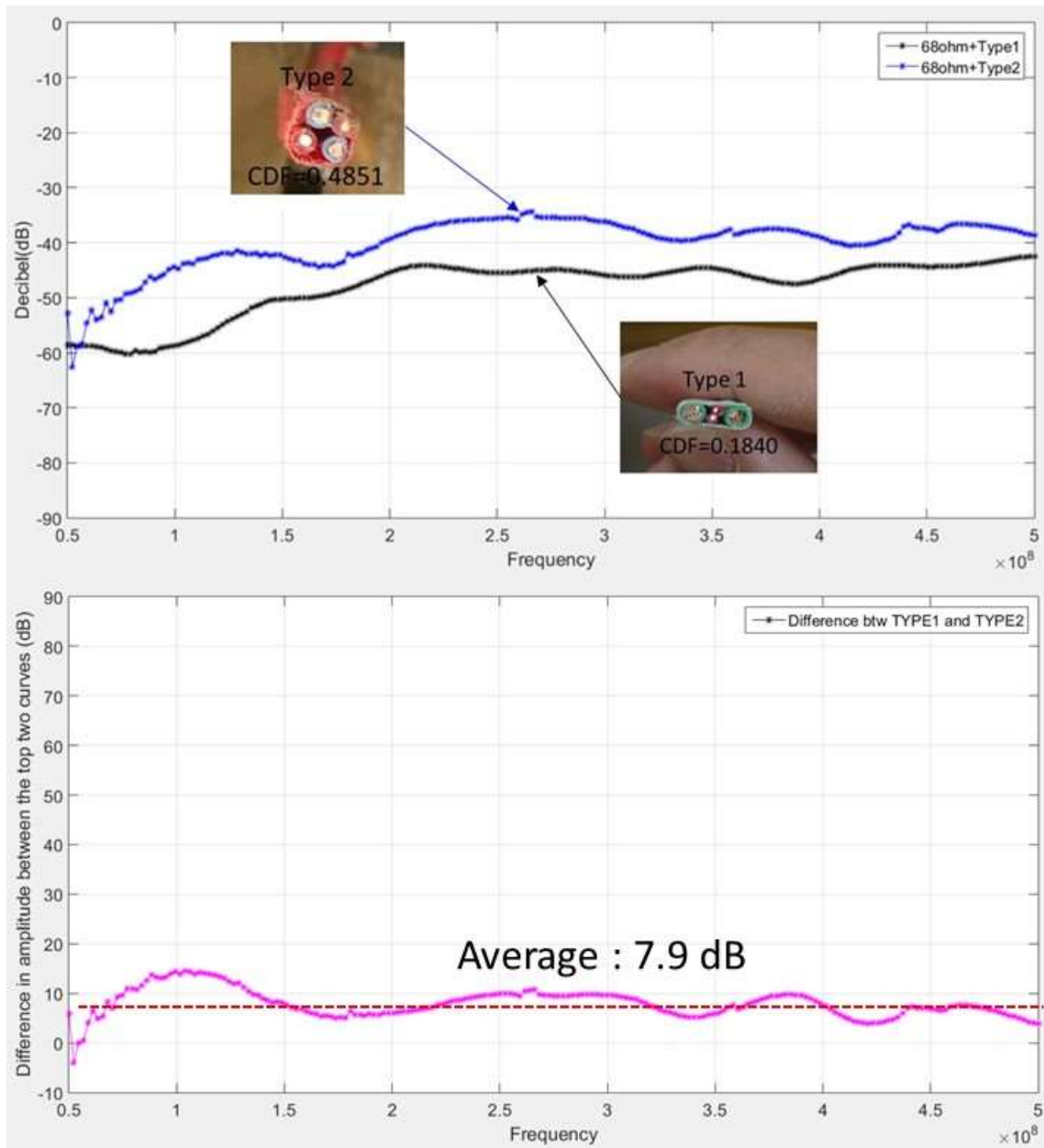


Fig. 1.11. The results of antenna mode currents in two wire harnesses

The two curves in the upper plot in Fig. 1.11 show the measured common-mode currents obtained with the two wire harnesses relative to the signal input (S_{21} on the network analyzer) as a function of frequency. The lower plot shows the difference between the two curves in the upper plot. As expected, the ratio of antenna mode currents averages

about 7.9 dB. There are some fluctuations due to the slightly different harness resonances, but the results show that common-mode currents are proportional to the change in the current division factor.

1.5 Conclusion

Matching the imbalance of a wire harness to the imbalance of its source and termination reduces the amount of common-mode current induced on the harness. A method for determining the imbalance (CDF) of wire harnesses using a simple electric-field solver has been presented. Wire harnesses with a pair of signal wires surrounded by thicker “ground” or return wires were shown to be capable of having CDFs comparable to typical printed circuit board configurations with a pair of signal traces over a return plane.

Measurements of two harness configurations demonstrated that common-mode currents are proportional to the changes in the current division factor. It is worth noting that the “ground” wires in these simulations and measurements do not have to literally connect to ground. For the purposes of determining the CDF, any wires in the harness that can freely carry current are “ground” wires. This includes wires that may be carrying currents associated with other signals in the harness.

References

- [1] D. Crolla, *Encyclopedia of Automotive Engineering*. John Wiley & Sons, 2015.
- [2] G. Andrieu, A. Reineix, X. Bunlon, J.-P. Parmantier, L. Kone, and B. Demoulin, “Extension of the Equivalent Cable Bundle Method for Modeling Electromagnetic Emissions of Complex Cable Bundles,” *IEEE Trans. Electromagn. Compat.*, vol. 51, no. 1, pp. 108–118, 2009.
- [3] T. Watanabe, O. Wada, T. Miyashita, and R. Koga, “Common-mode-current generation caused by difference of unbalance of transmission lines on a printed circuit board with narrow ground pattern,” *IEICE Trans. Commun.*, vol. 83, no. 3, pp. 593–599, 2000.

- [4] T. Watanabe, H. Fujihara, O. Wada, R. Koga, and Y. Kami, "A prediction method of common-mode excitation on a printed circuit board having a signal trace near the ground edge," *IEICE Trans. Commun.*, vol. 87, no. 8, pp. 2327–2334, 2004.
- [5] L. Niu and T. H. Hubing, "Rigorous Derivation of Imbalance Difference Theory for Modeling Radiated Emission Problems," *IEEE Trans. Electromagn. Compat.*, vol. 57, no. 5, pp. 1021–1026, 2015.
- [6] L. Niu and T. H. Hubing, "Modeling the Conversion between Differential Mode and Common Mode Propagation in Transmission Lines," *Clemson Veh. Electron. Lab. Tech. Rep. CVEL-14-055*, 2015.
- [7] C. R. Paul, *Introduction to electromagnetic compatibility*, vol. 184. John Wiley & Sons, 2006.

CHAPTER TWO

EVALUATION OF THE COMMON MODE VOLTAGE GENERATED BY DIFFERENT CAN TRANSCEIVERS

Abstract

Controller Area Network (CAN) signaling is differential; however unintended common-mode components of the signal can contribute to conducted and radiated emissions problems. In this report, five CAN transceivers are evaluated to determine how much common-mode voltage they produce in various circumstances.

2.1 Introduction

The common-mode (CM) component of differential signals often plays a key role in unintended conducted and radiated emissions. The pseudo-differential drivers generally used to produce balanced digital signals create a CM voltage component whenever the timing of the high-to-low and low-to-high transitions is not exactly the same.

Controller Area Network (CAN) is a network protocol widely used in the automotive industry. CAN employs analog circuit techniques to provide data transfers up to 1 Mb/s, and is a relatively low cost, low power networking option that has good noise immunity [1]. Researchers have investigated the electromagnetic immunity of CAN transceivers, and developed circuit-modeling procedures for signal immunity simulation [2]-[5]; but the electromagnetic emissions from modern CAN sources has not been extensively investigated. Many automotive electronics suppliers offer CAN transceivers that meet the specifications of the CAN standard [6]. However CAN transceivers from

different OEMs can exhibit significant differences in important characteristics not specified by the standard such as maximum slew rate and CM voltage.

Differential voltages and currents produce fields that are largely self-canceling, thus they are not good sources of conducted and radiated emissions [2]. On the other hand, imbalances in the differential signaling can introduce CM components resulting in EMI problems [7]-[12]. An analysis of source imbalances in differential signaling was conducted by Chen et al [11]. Hans-Werner et al showed that the EMC of in-vehicle multiplex networks is largely determined by the EMC of the transceiver ICs [13]. This paper describes measurements comparing different CAN transceivers to evaluate sources of imbalance that produce common-mode components in their signal outputs.

2.2 Test Setup for Measuring CM Voltages by CAN drivers

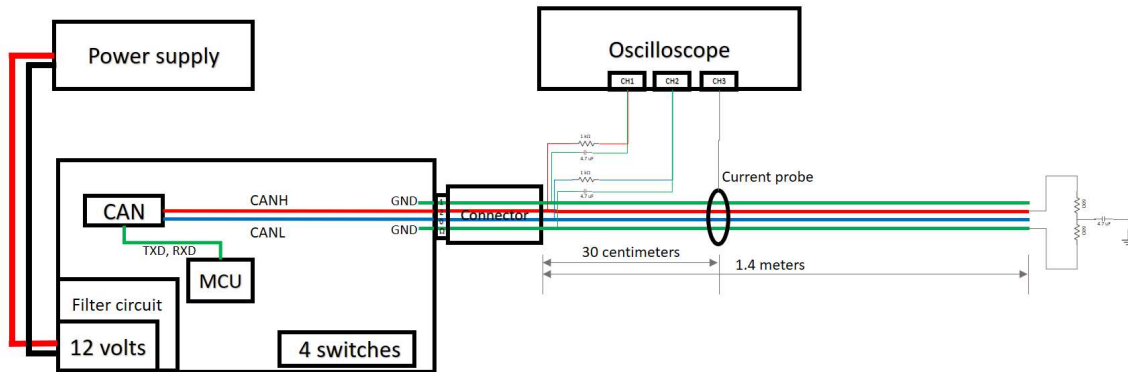


Fig. 2.1. Schematic diagram of CAN transceiver test set-up.

A test fixture was designed to evaluate the signals produced by various CAN transceivers. The test setup is schematically illustrated in Fig. 2.1. The CAN transceiver is mounted on a 20×15 cm printed circuit board (PCB). Five identical circuit boards were built; one for each transceiver evaluated. The PCBs were powered by an external 12-volt

DC supply. An NXP S912ZVC19F0MKHR microcontroller drives the transceiver. Four switches on each board are used to adjust the baud rate of the CAN transceiver. The differential signal traces, CANH and CANL, are routed across the board to a D-sub connector. The 5-volt power to the transceiver is supplied by the microcontroller. A 1.4-meter wire harness consisting of a twisted wire pair and two ground wires is attached to the D-sub connector. A 120-ohm differential termination is located on the wire harness at the connector. Another 120-ohm split termination (two 60-ohm resistors to ground) is located at the far end of the twisted wire pair.

A Fischer Custom Communications current probe (F-33-1) was used to measure CM current on the twisted wire pair. The CM current was measured 30 centimeters away from the connector. 21:1 probes for measuring the differential signals were built into the connector assembly. The probes consisted of 1-kohm resistors in series with the 50-ohm coaxial cables attached to the oscilloscope. The shields of the coaxial cables were connected to circuit ground through 4.7 uF capacitors to prevent low-frequency signal currents from returning through the oscilloscope ground. The probes were integrated with the connector assembly so that each transceiver board could be measured using the same probes.

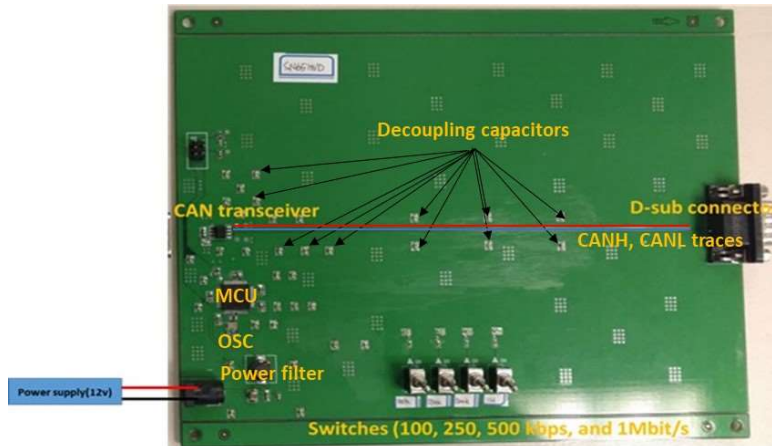


Fig. 2.2. The fabricated printed circuit board top view

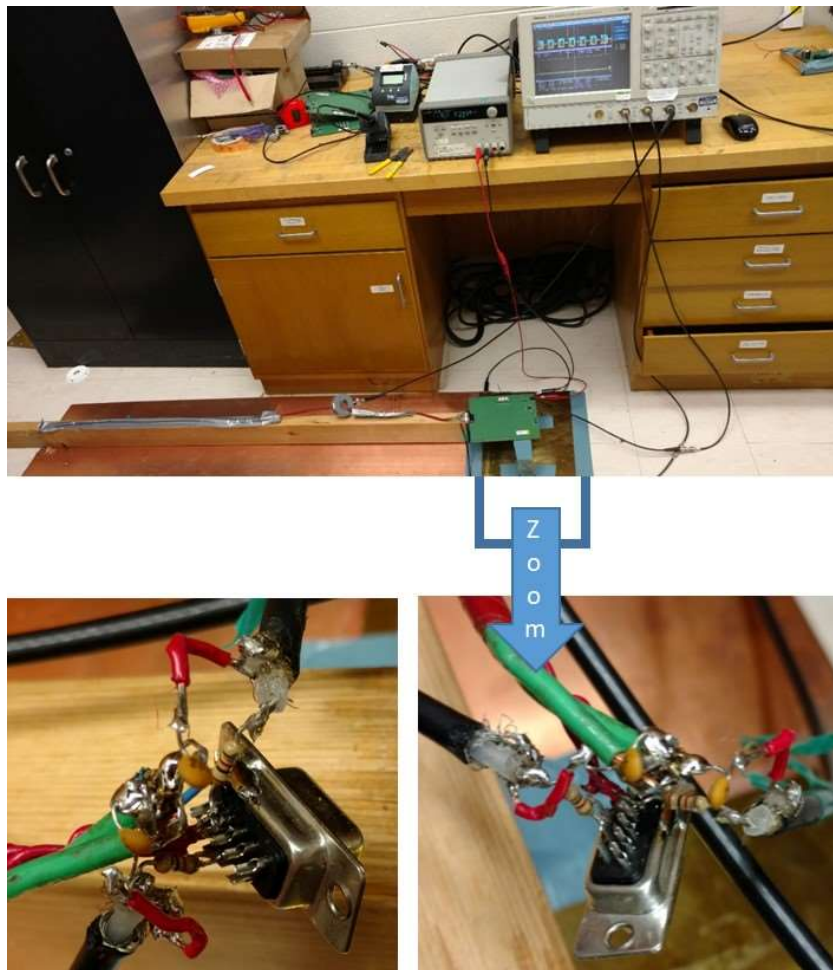


Fig. 2.3. Test set-up and probe connection configuration

The PCB and the test set-up are shown in Fig. 2.2 and Fig. 2.3, respectively. Forty decoupling capacitors are mounted on the PCB to minimize power-bus noise. Four switches on the PCB are used to set the baud rate to 100 kb/s, 250 kb/s, 500 kb/s, or 1 Mb/s. Five PCBs were fabricated with exactly the same design. Five CAN transceivers were selected with identical packaging: “A” and “B” from the same company, “C”, “D”, and “E” from three other companies. The wire harness consisted of a twisted wire pair (AWG18) and two ground wires (AWG12). The length of the wire harness was 1.4 m and the differential signal traces on the PCB were 17 cm long. The voltage on each of the wires in the twisted pair (relative to ground) was measured at the connector.

2.3 Experiment Results

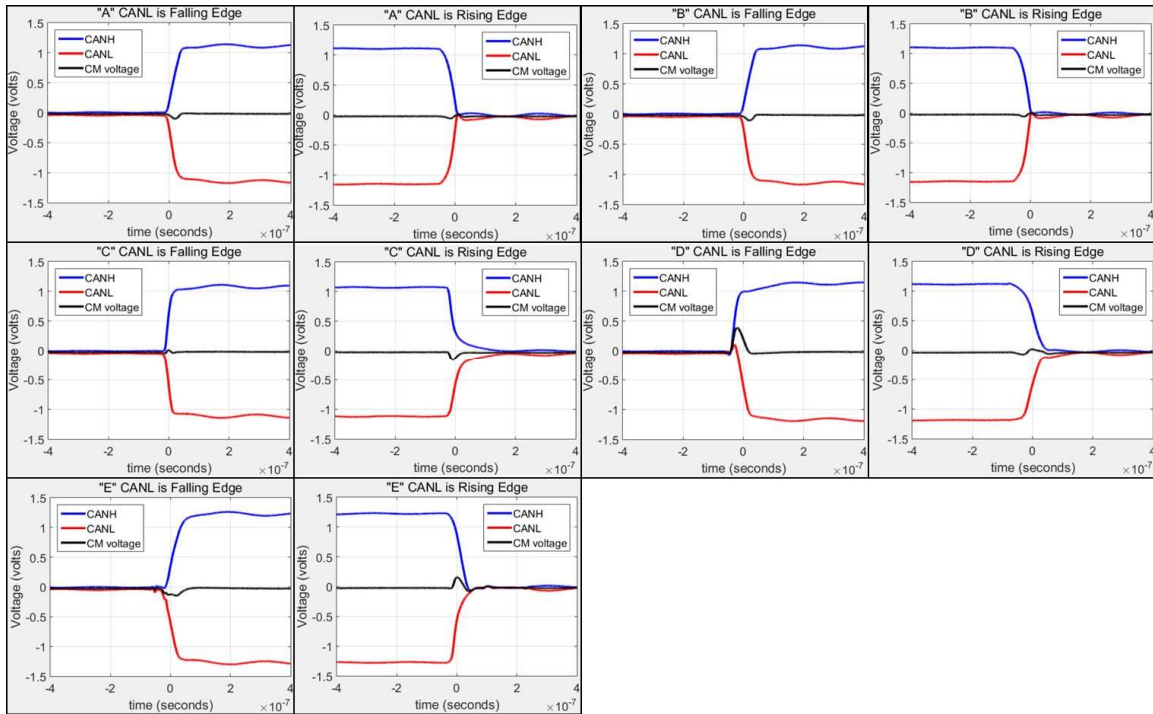


Fig. 2.4. Measured differential signal voltage and CM voltage for the five transceivers

Nominally, the CM voltage in a CAN signal is a constant DC value of approximately 2.5 volts. In these measurements, the 4.7-uF capacitor filters out the DC component of the CM voltage. Nonzero fluctuations in the CM component of the signal arise due to signal asymmetries such as amplitude mismatches between V_1 and V_2 rise- and fall-time mismatches, or time offsets between the transitions of the two single-ended signals (skew) [10].

The voltages measured on the CANH and CANL wires for each of the transceivers are shown in Fig. 2.4. The sum of these voltages, the common-mode voltage, is also shown. The baud rate in this case is 1 Mb/s, which is the highest speed for the given transceivers. The CM voltage is the highest at the time of the transition of the differential voltage. The measured differential signal voltages are approximately 0 or 2.2 volts, depending on the state of the output. In this test, the “A” and “B” transceivers generate smaller CM voltages than the other transceivers because their signals are more symmetric. Generally, the amplitude of the CM voltage was different on low-to-high transitions than it was on high-to-low transitions. This was particularly the case with the “D” transceiver.

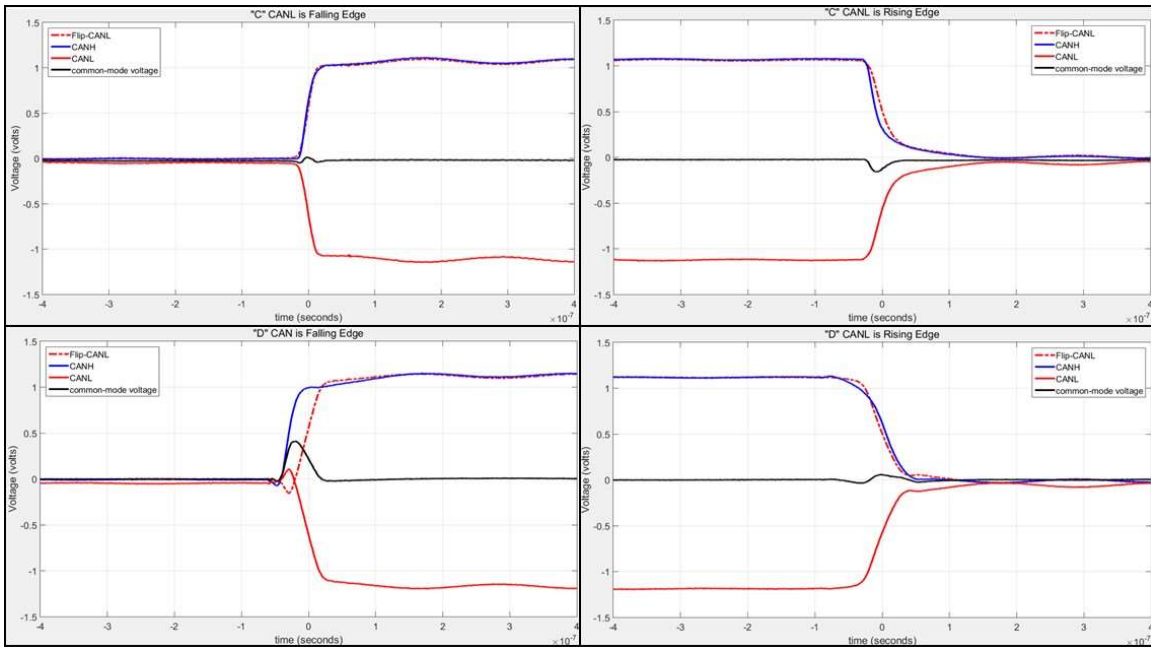


Fig. 2.5. Slew rates and time offset in the transition

Fig. 2.5 shows the differential signals for the “C” and “D” transceivers with the CANL signal inverted to illustrate differences in the timing and slew-rate that result in the CM voltage. The dominant source of CM voltage in the “A”, “B” and “C” transceivers was the difference in the slew rates. The “D” transceiver, however, has a time offset between transitions when CANL is falling. That is resulted in the worst CM voltage generated by any of the five transceivers evaluated.

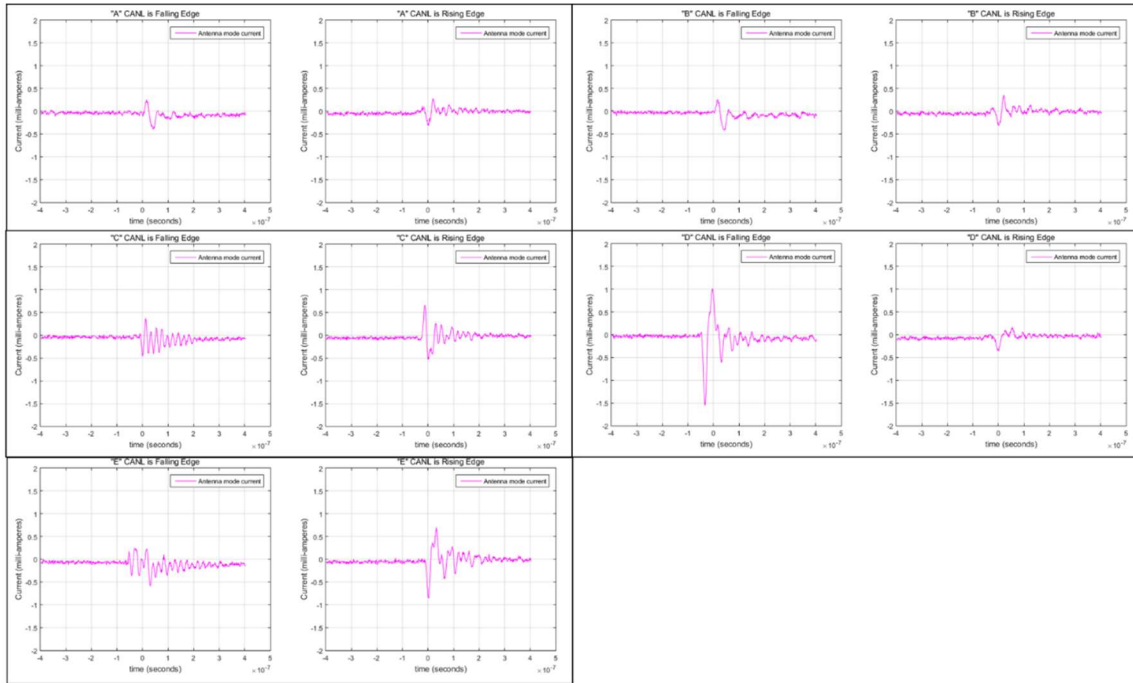


Fig. 2.6. CM currents measurements for the five transceivers

The CM voltage on the twisted wire pair produces a CM current. The CM current measured with the F-33-1 probe for each transceiver on both rising and falling transitions is shown in Fig. 2.6. The baud rate is 1 Mb/s.

The peak CM current for each transceiver was recorded. For example, as indicated in the plots, the peak value of the measured CM current is -0.48 mA for transceiver “A” on the rising edge and 0.44 mA for transceiver “B” on the falling edge. The fall time of the “C” transceiver is much faster than the other transceivers, so even though the peak CM voltage is not high, the energy in the CM voltage waveform is high enough to generate significant CM current.

Generally, the results show that higher CM voltages generated higher CM currents. The ringing in the CM current waveforms is due to the CM impedance of the wire harness structure, which is largely determined by the length of the harness and its CM terminations.

Table 2.1. Measured transition times and CM voltage peaks and CM current peaks

CANL is falling edge		Rising/Falling time	CM voltage (pk)	CM Currents (pk)	CANL is rising edge		Rising/Falling time	CM voltage (pk)	CM Currents (pk)
"A"	100kHz	37 ns / 39 ns	-88 mV	0.44 mA	"A"	100kHz	35 ns / 37 ns	-39 mV	-0.48 mA
	250kHz	37 ns / 39 ns	-89 mV	0.42 mA		250kHz	34 ns / 37 ns	40 mV	-0.47 mA
	500kHz	38 ns / 34 ns	-84 mV	0.43 mA		500kHz	34 ns / 37 ns	-41 mV	-0.47 mA
	1 MHz	38 ns / 34 ns	-83 mV	0.43 mA		1 MHz	35 ns / 38 ns	-39 mV	-0.48 mA
"B"	100kHz	37 ns / 33 ns	-95 mV	0.44 mA	"B"	100kHz	36 ns / 38 ns	-35 mV	-0.43 mA
	250kHz	38 ns / 34 ns	-95 mV	0.44 mA		250kHz	35 ns / 37 ns	-35 mV	-0.46 mA
	500kHz	38 ns / 40 ns	-92 mV	0.46 mA		500kHz	35 ns / 38 ns	38 mV	-0.46 mA
	1 MHz	39 ns / 34 ns	-87 mV	0.48 mA		1 MHz	35 ns / 38 ns	37 mV	-0.47 mA
"C"	100kHz	27 ns / 20 ns	61 mV	-0.77 mA	"C"	100kHz	70 ns / 64 ns	-134 mV	0.66 mA
	250kHz	26 ns / 23 ns	50 mV	-0.70 mA		250kHz	69 ns / 70 ns	-135 mV	0.66 mA
	500kHz	26 ns / 21 ns	46 mV	0.68 mA		500kHz	71 ns / 60 ns	-134 mV	0.66 mA
	1 MHz	22 ns / 24 ns	38 mV	0.69 mA		1 MHz	62 ns / 66 ns	-135 mV	0.66 mA
"D"	100kHz	85 ns / 39 ns	424 mV	1.5 mA	"D"	100kHz	52 ns / 67 ns	52 mV	-0.34 mA
	250kHz	84 ns / 38 ns	419 mV	1.5 mA		250kHz	52 ns / 70 ns	55 mV	-0.32 mA
	500kHz	86 ns / 39 ns	416 mV	1.6 mA		500kHz	53 ns / 67 ns	53 mV	-0.35 mA
	1 MHz	81 ns / 38 ns	413 mV	1.5 mA		1 MHz	57 ns / 67 ns	59 mV	-0.34 mA
"E"	100kHz	52 ns / 49 ns	-124 mV	-0.39 mA	"E"	100kHz	50 ns / 44 ns	-185 mV	-0.95 mA
	250kHz	53 ns / 47 ns	-122 mV	-0.38 mA		250kHz	50 ns / 44 ns	-184 mV	-0.93 mA
	500kHz	52 ns / 45 ns	-124 mV	-0.38 mA		500kHz	51 ns / 44 ns	-182 mV	-0.96 mA
	1 MHz	52 ns / 50 ns	-125 mV	-0.44 mA		1 MHz	51 ns / 43 ns	-183 mV	-0.95 mA

Similar measurements were made on each transceiver at each of the four baud rates and the results are summarized in Table 2.1. Each CAN transceiver tested produced a differential signal complying with the CAN standard [14]. Each transceiver tested appeared to control the rise and fall times of the signal, which ranged from 20 nsec to 86 nsec. Nevertheless, on some transceivers the rise-times were significantly different from the fall-times. Peak CM voltage magnitudes ranged from 35 mV to 419 mV, and peak CM current magnitudes ranged from 0.32 mA to 1.6 mA.

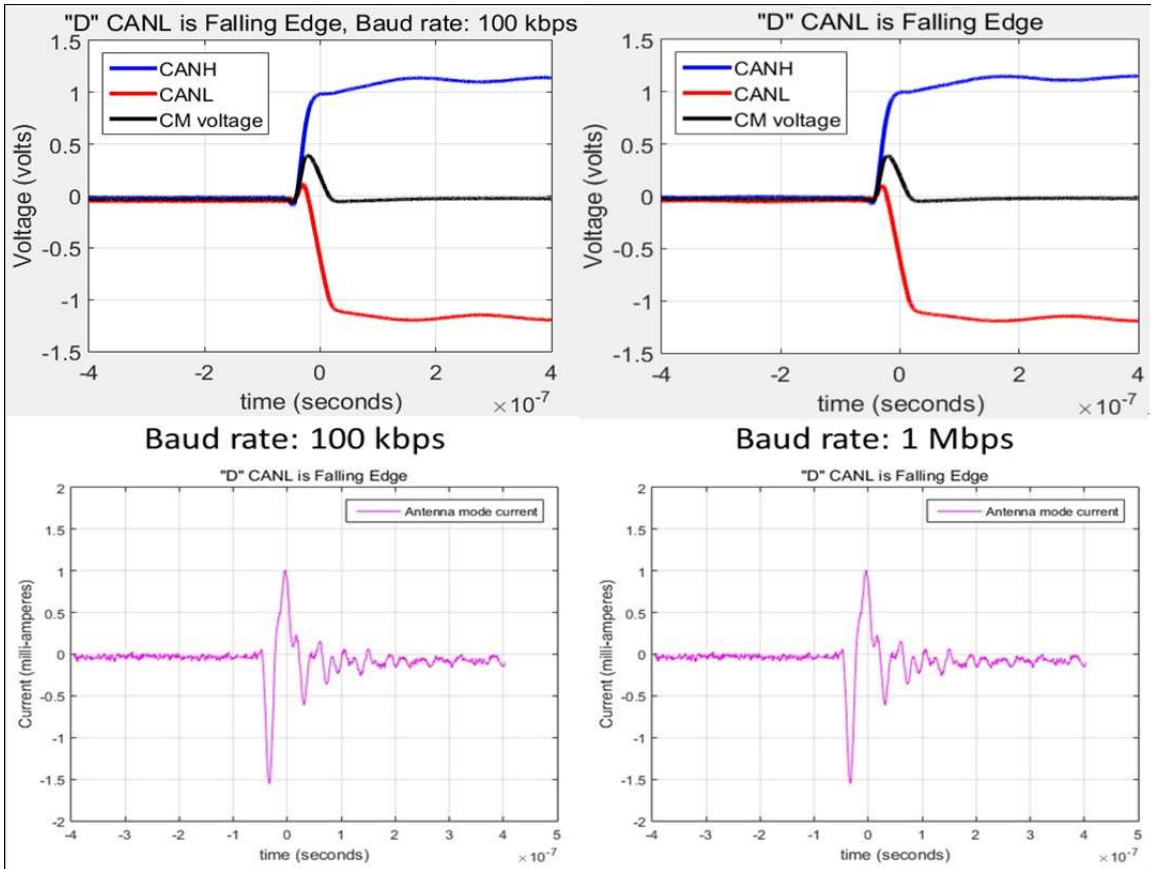


Fig. 2.7. CM voltages and currents at different baud rates

No significant difference in the CM voltages or currents was observed when varying the baud rate of a given transceiver. For example, Fig. 2.7 shows the waveforms measured on transceiver “D” at 100 kbps and 1 Mbps.

Baud rate: 1 Mbps, step frequency: 1.25 MHz

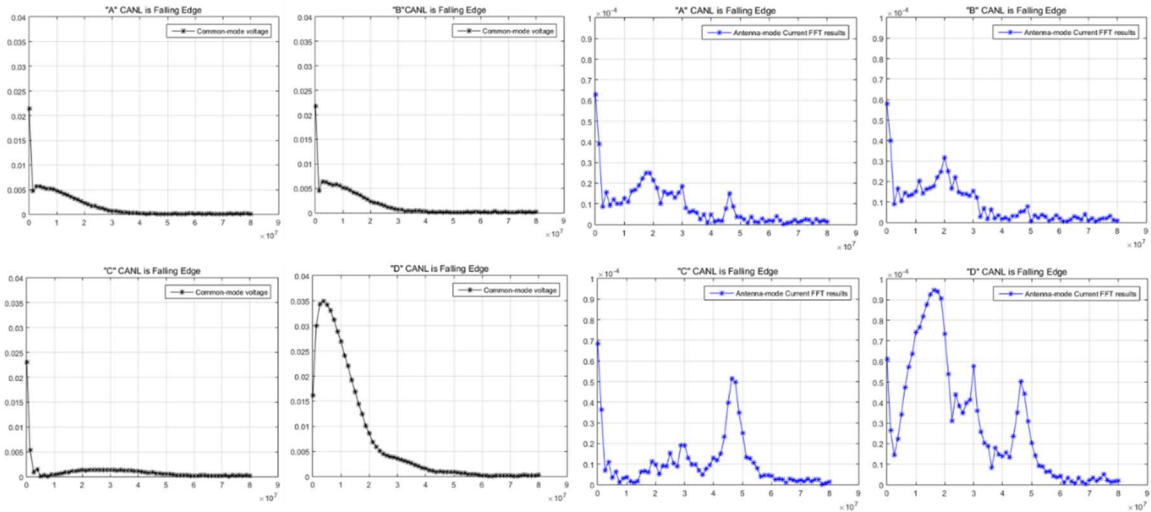


Fig. 2.8. Frequency domain representation of the CM voltages and currents

The Fourier transform (FFT) of the CM voltage and current waveforms was calculated for four of the measured waveforms and is shown in Fig. 2.8. The CM currents exhibit peaks at frequencies corresponding to resonances of the wire harness. When the CM voltage is strong enough to excite the wire harness, the corresponding CM currents peaks appear at the resonant frequencies. The “A” and “B” transceivers generate CM voltages that have more energy at 20 MHz than they do at 40 MHz and higher. These pulses excite a system resonance at around 20 MHz. The “C” and “D” transceivers generate CM pulses with significant energy above 40 MHz and excite a system resonance at around 46 MHz. On the CANL falling edge, the “D” transceiver exhibited a timing offset that generated significant low-frequency energy. This drives the resonance just below 20 MHz much more strongly than the other pulses.

2.4 Conclusion

In this paper, the CM voltages generated by five different CAN transceivers were evaluated. All of the transceivers met the functional requirements of the CAN specification. Each of the transceivers appeared to control the rise and fall times, which ranged from 20 nsec to 86 nsec. Some transceivers did a poor job of matching the rise and fall times resulting in significant common-mode voltage fluctuations during transitions. The CM voltage fluctuations did not appear to be dependent on the baud rate. The analysis of the common-mode currents indicates that the resonant frequencies were mainly determined by the CM impedance of the harness, not by the common-mode fluctuations, which tended to be relatively wide-band pulses. Nevertheless, the frequency content of the CM voltages did influence which system resonances were excited most strongly.

References

- [1] H. Bauer, *Automotive Electrics/Automotive Electronics*. vol. 4, John Wiley & Sons, 2004.
- [2] M. Fontana, F. G. Canavero and R. Perraud, "Integrated circuit modeling for noise susceptibility prediction in communication networks," *IEEE Trans. Electromagn. Compat.*, vol. 57, no.3, pp. 339-348, 2015.
- [3] J. Koo et al, "A nonlinear microcontroller power distribution network model for the characterization of immunity to electrical fast transients," *IEEE Trans. Electromagn. Compat.*, vol. 51, no.3, pp. 611-619, 2009.
- [4] J. Zhang et al, "Modeling of the immunity of ICs to EFTs," in *Electromagnetic Compatibility (EMC), 2010 IEEE International Symposium On*, 2010.
- [5] M. Fontana and T. H. Hubing, "Characterization of CAN network susceptibility to EFT transient noise," *IEEE Trans. Electromagn. Compat.*, vol. 57, no.2, pp. 188-194, 2015.
- [6] International Electrotechnical Commission, "CISPR 25 limits and methods of measurement of radio disturbance characteristics for the protection of receivers used on board vehicles," Geneva: International Electrotechnical Commission, 1995.

- [7] B. Archambeault et al, "Electromagnetic radiation resulting from PCB/high-density connector interfaces," *IEEE Trans. Electromagn. Compat.*, vol. 55, no.4, pp. 614-623, 2013.
- [8] L. Niu and T. H. Hubing, "Rigorous derivation of imbalance difference theory for modeling radiated emission problems," *IEEE Trans. Electromagn. Compat.*, vol. 57, no.5, pp. 1021-1026, 2015.
- [9] M. Sørensen, T. H. Hubing and K. Jensen, "Study of the impact of board orientation on radiated emissions due to common-mode currents on attached cables," in *Electromagnetic Compatibility (EMC), 2016 IEEE International Symposium On*, 2016, .
- [10] C. R. Paul, "A comparison of the contributions of common-mode and differential-mode currents in radiated emissions," *IEEE Trans. Electromagn. Compat.*, vol. 31, no.2, pp. 189-193, 1989.
- [11] C. Wang and J. L. Drewniak, "Quantifying the effects on EMI and SI of source imbalances in differential signaling," in *Electromagnetic Compatibility, 2003 IEEE International Symposium On*, 2003.
- [12] H. Kwak and T. H. Hubing, "Investigation of the imbalance difference model and its application to various circuit board and cable geometries," in *Electromagnetic Compatibility (EMC), 2012 IEEE International Symposium On*, 2012.
- [13] H. Luetjens and H. Eisele, "How to qualify EMC in multiplexing," SAE International, 1999.
- [14] R. Bosch, "CAN specification version 2.0," 1991.

CHAPTER THREE

EFFECT OF GROUND PROXIMITY ON COMMON-MODE CURRENTS IN WIRE HARNESSSES

Abstract

Common-mode currents are the most significant source of radiated emissions from wire harnesses. Differential-mode signals are converted to common-mode currents whenever the electrical balance of the wire harness changes. Wire harnesses may experience a change in their electrical balance when the distance from the wire harness to the ground structure changes. This paper explores the effect of ground proximity on the induced common-mode currents in wire harnesses.

3.1 Introduction

Common-mode currents play a key role in unintentional radiated emissions. Clayton Paul [1] and many others have demonstrated that common-mode currents radiate much more effectively than differential-mode currents. Conversion from differential mode to common mode occurs when there is a change in the electrical balance of a transmission line. The key to preventing differential-mode signals from inducing common-mode currents is maintaining the same level of electrical balance or imbalance all the way from the signal source to the signal termination.

An imbalance difference model describing how differential- to common-mode conversion occurs resulting in radiated emissions was first introduced by Watanabe et al. [2], [3]. It was later rigorously derived and validated by Niu et al. [4]. Niu demonstrated that imbalance difference calculations are exact provided that the imbalance factor, h ,

represents the actual ratio of currents on the two transmission line conductors excited by a common-mode source.

In [5], the author demonstrates that placing extra ground on the other side of a signal trace in a printed circuit board reduces the radiation emissions. This paper provided insight about the importance of ground proximity, without directly referencing electrical imbalance.

Changyi Su et al. [6] demonstrated how to apply the imbalance difference model to the analysis of radiation from circuit boards due to signal trace terminations. Several other authors have also demonstrated useful ways of applying the imbalance difference method to estimate the radiated emissions from circuit board geometries [7]–[12]. Tetsushi Watanabe et al. [13], [14] estimated radiated emissions due to the common-mode currents caused by a signal line in the vicinity of the ground plane edge on a PCB.

These papers showed that ground proximity and asymmetric geometries affect electrical balance changes resulting in common-mode currents.



Fig. 3.1. Wire harnesses in an automobile.

It is common practice to use wire harnesses to carry electronic signals in metallic structures such as automobiles as shown in Fig. 3.1. The relative location of wires change

as they move through the harness and some wires may peel off and go in a different direction from other wires in the harness. Sometimes the harness is run in close proximity to the frame of the car, other times it's routed away from the frame. In other words, for any intentional or unintentional currents flowing on the wires in the harness and returning on the frame, automotive wire harnesses can experience significant changes in electrical balance. The wire harnesses typically have ground wires designed to provide a return path for high-frequency currents and reduce radiated emissions. However, the electrical balance of harnesses that have ground wires is still affected by changes in the proximity of the wire harness to the frame.

This paper explores the impact of wire harness proximity to ground on the generation of common-mode currents. Section 3.2 explains how to calculate the common-mode voltage from the differential-mode voltage for a given transmission line and describes a test setup for evaluating the effect of changes in the harness-to-frame proximity. Section 3.3 discusses the test results and validates the results using the imbalance difference method. Finally, the conclusions of the study are summarized in Section 3.4.

3.2 Wire Harness Geometry under Study

3.2.1 Conversion to common-mode voltage from differential-mode voltage

It is common to send differential signals through twisted wire pairs in a wiring harness. For example, controller area network (CAN) is a network widely used in the automotive industry. The CAN signaling is differential but common-mode currents flow on CAN wire pairs [15]. These common-mode currents don't result in significant radiated emissions if they return on another wire in the harness or on the nearby vehicle frame.

However, antenna mode currents that flow in one direction on all conductors play a key role in radiated emissions. These antenna mode currents are the result of changes in the imbalance of the transmission line [16]. A test set-up was designed to explore how the proximity of the vehicle frame effects the imbalance and the antenna-mode currents.

The wire harness in the test set up has three wires as shown in Fig. 3.2. Two of the wires are a twisted wire pair. Both wires in the pair carry current in the same direction, representing the unintentional common-mode current generated by a differential signal source such as a CAN transceiver. The third wire is a ground wire that serves as a return path for the currents flowing on the twisted wire pair. Any change in the imbalance factor observed by the signal currents propagating down the wire pair and returning on the ground wire will result in a voltage that drives antenna-mode current onto the structure [2, 4]. The driving voltage will be,

$$V_{AM} = \Delta h \times V_{CM} \quad (3.1)$$

where V_{AM} is the common-mode voltage driving the structure, Δh is the change in the imbalance factor, and V_{CM} is the differential-mode voltage in the transmission line [4]. To avoid confusion, we will use the term AM, instead of CM to describe currents that propagate in one direction on both conductors without returning on a nearby ground.

3.2.2 Description of the test setup

The geometry and cross-sectional view of the wire harness under study are illustrated in Fig. 3.2.

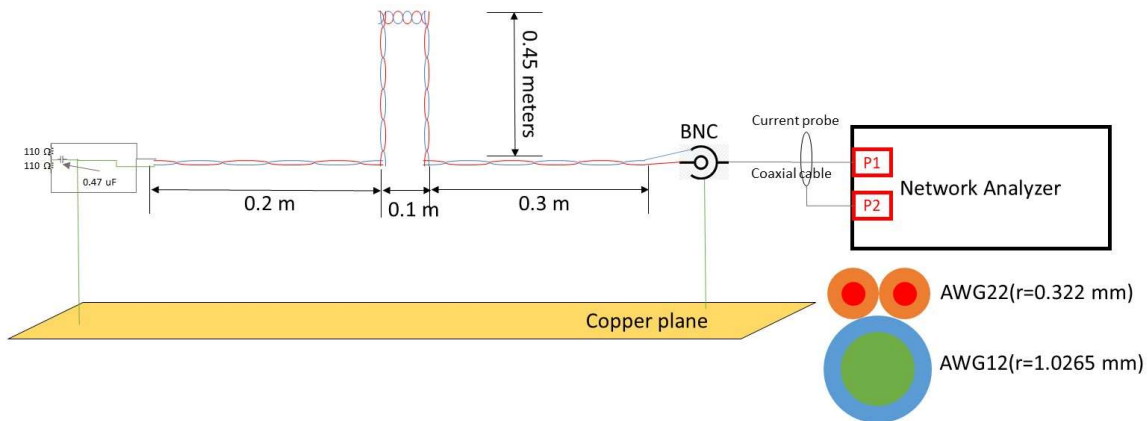


Fig. 3.2. Schematic view of the test environment and wire harness geometry

A network analyzer drives a signal down a coaxial cable. The analyzer and the cable are perfectly unbalanced (i.e. $h=0$). The network analyzer signal sweeps in frequency from 50 MHz to 450 MHz. The coaxial cable drives a wire harness. The center conductor of the coaxial cable connects simultaneously to both wires in a twisted wire pair. The shield of the coaxial cable connects to a larger “ground” wire in the harness. The analyzer signal simulates a common-mode current being driven on the twisted wire pair and returning on “ground” or other wires in the harness. A current probe is used to measure the antenna-mode current induced on the coaxial cable.

The twisted wire pair consists of two AWG22 wires. The “ground” wire is AWG12. The cross-sectional areas of the wires are 0.326 mm^2 for each of the AWG22 wires and 3.31 mm^2 for the ground wire. The wire insulation is polyvinyl chloride ($\epsilon_r = 3$). The wire harness was carefully made to maintain the same cross-sectional geometry from one end to the other. A copper plane was placed underneath the wire harness and the coaxial cable. A split termination load (two 110-ohm resistors to ground) was used to terminate the twisted wire pair at the load end. The CM impedance of the termination was 55 ohms in

order to nearly match the CM impedances of the wire harness and the coaxial cable. The ground plane was connected to the ground wire at both ends so the current could return either on the ground wire or the ground plane.

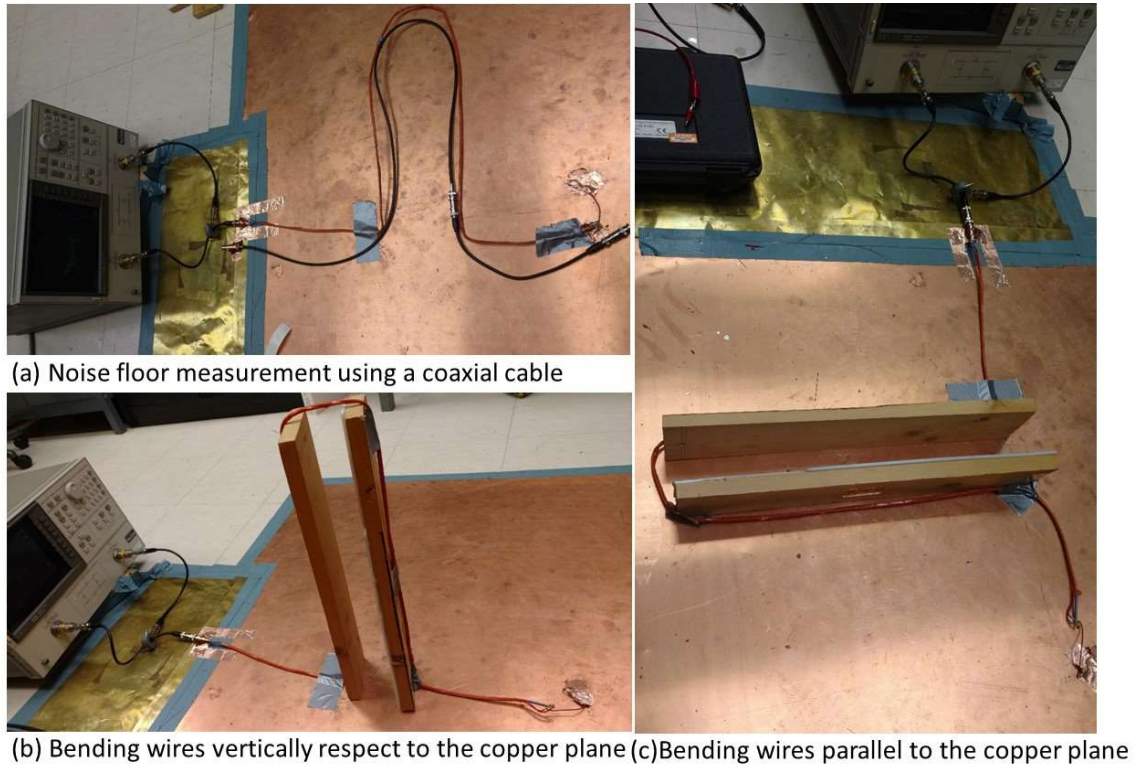


Fig. 3.3. Test setup for each bending configuration

Three configurations were tested, as shown in Fig. 3.3. To determine the level of common-mode current on the coaxial cable due to ambient noise sources, the wire harness was replaced with an equal length of coaxial cable as shown in Fig. 3.3.(a). In this configuration, there is no imbalance change and no reflected voltage at the load, because the cable is terminated by the matched impedance.

The other two configurations include the wire harness illustrated in Fig. 3.2. In both of these configurations, the wire harness extends for 30 cm, makes a 90-degree turn,

extends another 45 cm, turns back to the original direction and extends another 10 cm, turns 90 degrees again and back-tracks to its original axis, then extends another 30 cm to the termination. In one configuration, Fig. 3.3c, the harness maintains a constant proximity to the ground plane. In the other configuration, Fig. 3.3b, the harness starts and ends near the ground plane, but loses proximity to the plane in the middle.

3.3 Results and Discussion

The common-mode characteristic impedance of the wire harness was calculated using a 2D field solver. It varied depending on the harness proximity to the plane from 46 ohms to 56 ohms. Using the same 2D field solver, the imbalance factors were calculated. When the harness is in close proximity to the plane, the imbalance factor is $h = 0.0305$. When the harness is 45 cm above the plane, the imbalance factor is $h = 0.3863$.

The change in the imbalance factor at the interface between the coaxial cable and wire harness equals the imbalance factor of the wire harness. When the wire harness maintains its proximity to the plane, this is the only source of antenna-mode current driving the coaxial cable.

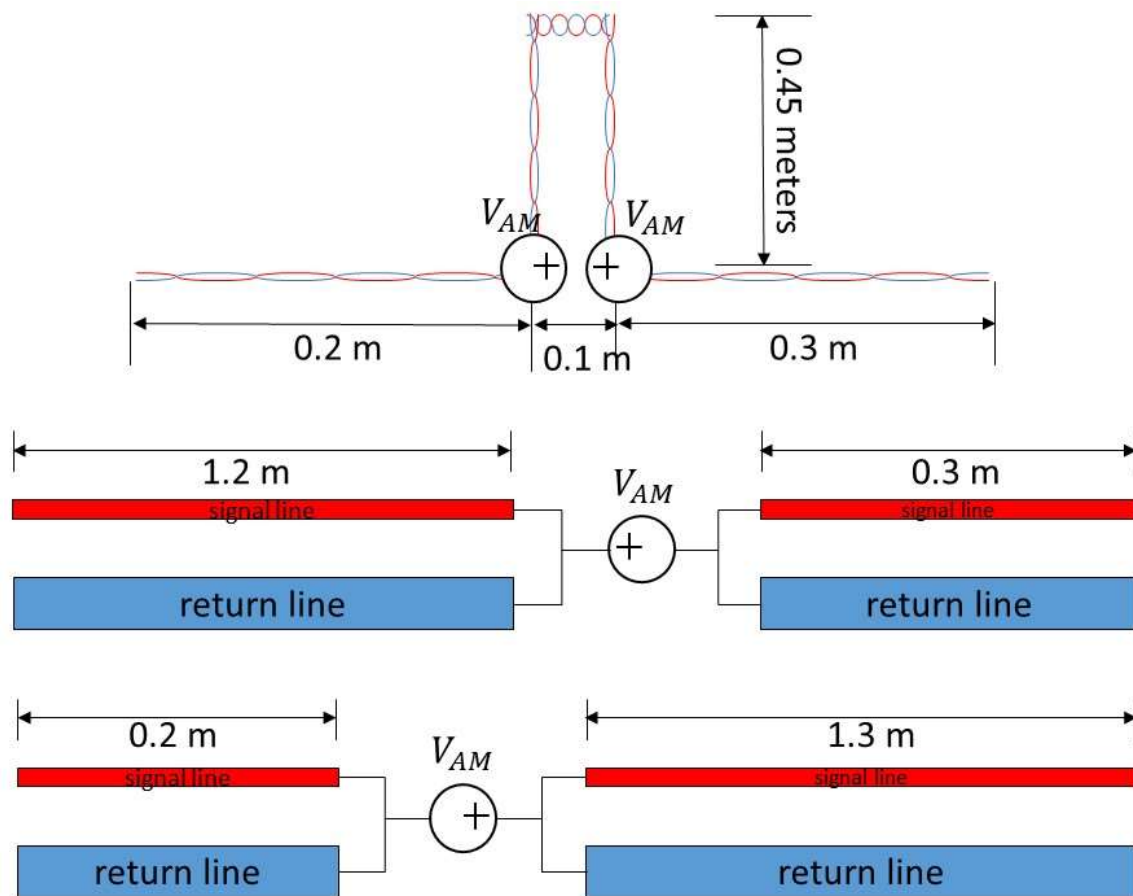


Fig. 3.4. Common-mode excitation on the vertically bended wire harness

When the harness loses its proximity to the plane then gets it back again, two more sources of antenna-mode current with opposite polarities are created as shown in Fig. 3.4. The amplitude of the antenna-mode current due to the voltages at the two vertical bends is not easily calculated because the antenna is a complex geometry that includes the coaxial cable, network analyzer, etc. However, analyzing the average input impedance at the each voltage source allows one to estimate the average antenna-mode current due to the combination of the two sources.

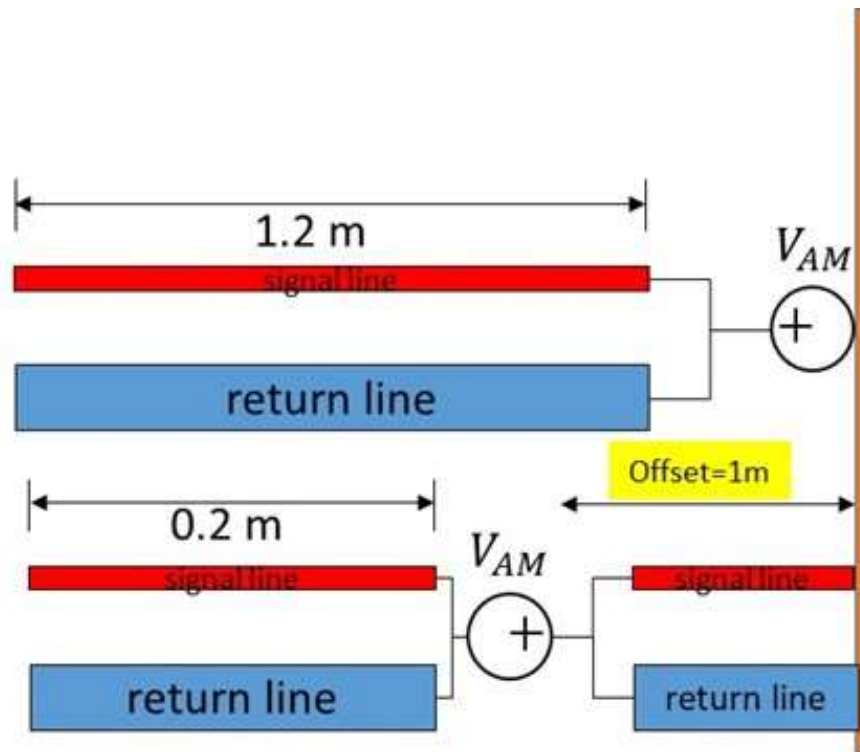


Fig. 3.5. The quarter-wave monopole antenna modelling

In Fig. 3.5, the right half of the wire harness, coaxial cable, network analyzer and building ground structure are represented by an infinite ground plane. The source at the first bend drives the left half of the harness relative to this plane. The second source is offset from the first, closer to the end of the structure.

The offset position (z) is 1 meter from the center of the monopole and the length of the monopole (l) is 1.2 meters. On average, the input impedance of the second source is higher than the input impedance of the first source, because of its proximity to the end of the harness. To estimate the relative input impedance of the voltage sources, a full-wave simulation is performed by FEKO.

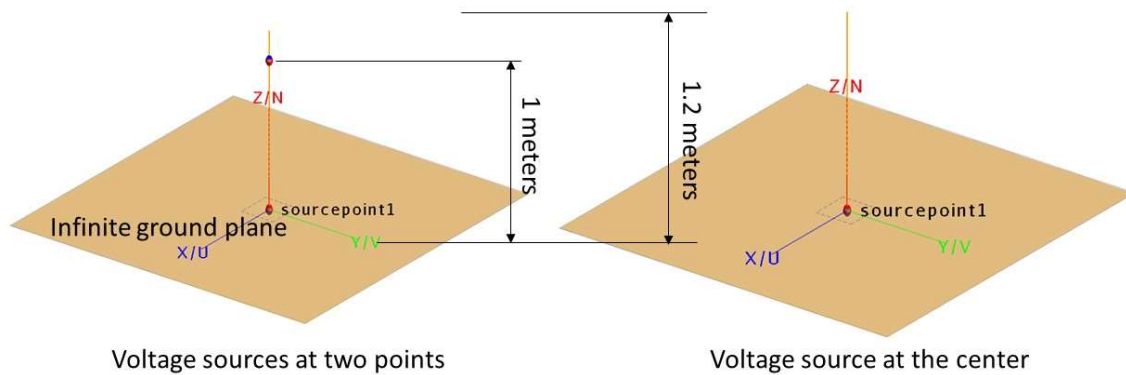


Fig 3.6. Full-wave simulation configuration

The full-wave simulation test setup is shown in Fig.3.6. The monopole antenna has two voltage sources, one at the center of the monopole antenna and one that is 1 meter away from the center. The second voltage source is 180 degrees out of phase with the first one.

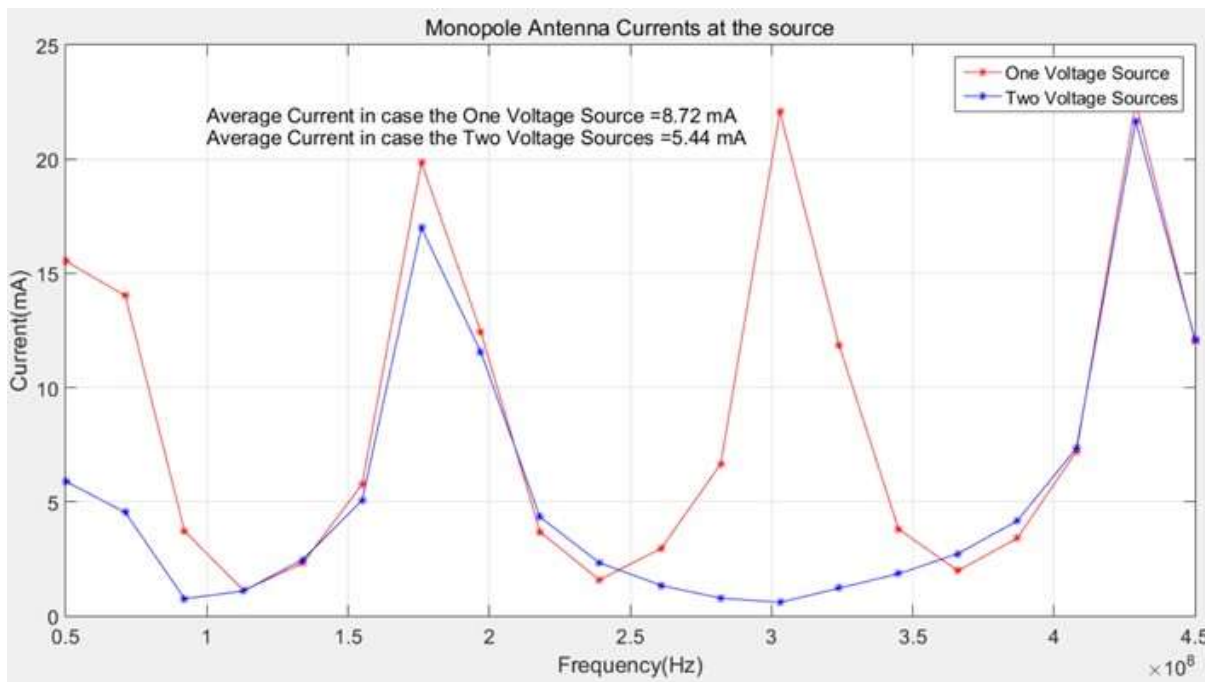


Fig. 3.7. FEKO results for the antenna-mode currents at the lower voltage source

The calculated antenna-mode current magnitude at the lower source position is plotted in Fig. 3.7. The red curve is the current on the wire with only the lower source active. The blue curve is the current with both sources active.

The magnitude of the current with both sources averaged over this frequency range is 5.44 mA (74.7 dB(μ A)). The average value of the current with only the lower source is 8.72 mA (78.8 dB(μ A)). Therefore, we expect the average antenna-mode current from the two vertical bends in our test set-up to be approximately 4 dB lower than the average current that would be induced by the first bend only.

Therefore when the harness is lying flat over the ground plane, we expect to see only one antenna-mode source (at the junction of the coax to the harness). That source has an amplitude of

$$\begin{aligned} h_{coax} &= 0 \\ \Delta h_{\parallel} &= 0.0305 \\ V_{AM\parallel} &= \Delta h_{\parallel} \times V_{CM} \end{aligned} \tag{3.2}$$

where V_{CM} is the amplitude of the common-mode voltage at input to the harness. The imbalance factor of the coaxial cable (h_{coax}) is zero because the cable is perfectly unbalanced. The imbalance factor difference at the interface with coaxial cable to the wire harness is then the imbalance factor of the wire harnesses bended parallel ($h_{\parallel} = 0.0305$).

With the harness raised vertically above the ground plane as shown in Fig. 3.3b, two additional antenna-mode sources are introduced. The average amplitude of these sources together is,

$$\begin{aligned}
h_{\parallel} &= 0.0305 \\
h_{\perp} &= 0.3863 \\
V_{AM\perp} &= (h_{\perp} - h_{\parallel})V_{CM} = 0.3558V_{CM} \quad \leftarrow \text{first source} \\
V_{AM2\perp} &= \frac{5.44 \text{ mA}}{8.72 \text{ mA}} V_{AM\perp} = 0.222V_{CM} \quad \leftarrow \text{both sources}
\end{aligned} \tag{3.3}$$

Note that the antenna-mode voltage generated by the two vertical bends is much higher than the antenna-mode voltage generated by the coax-to-harness transition. Assuming the common-mode voltage is approximately the same at both places, the ratio is

$$20 \log \left(\frac{V_{AM2\perp}}{V_{AM\parallel}} \right) = 20 \log \left(\frac{0.222 V_{CM}}{0.0305 V_{CM}} \right) = 17 \text{ dB} \tag{3.4}$$

Therefore, on average, the magnitude of the antenna-mode current for the configuration with the two vertical bends should be significantly higher than the magnitude of the current on the harness that maintains its proximity to the ground plane.

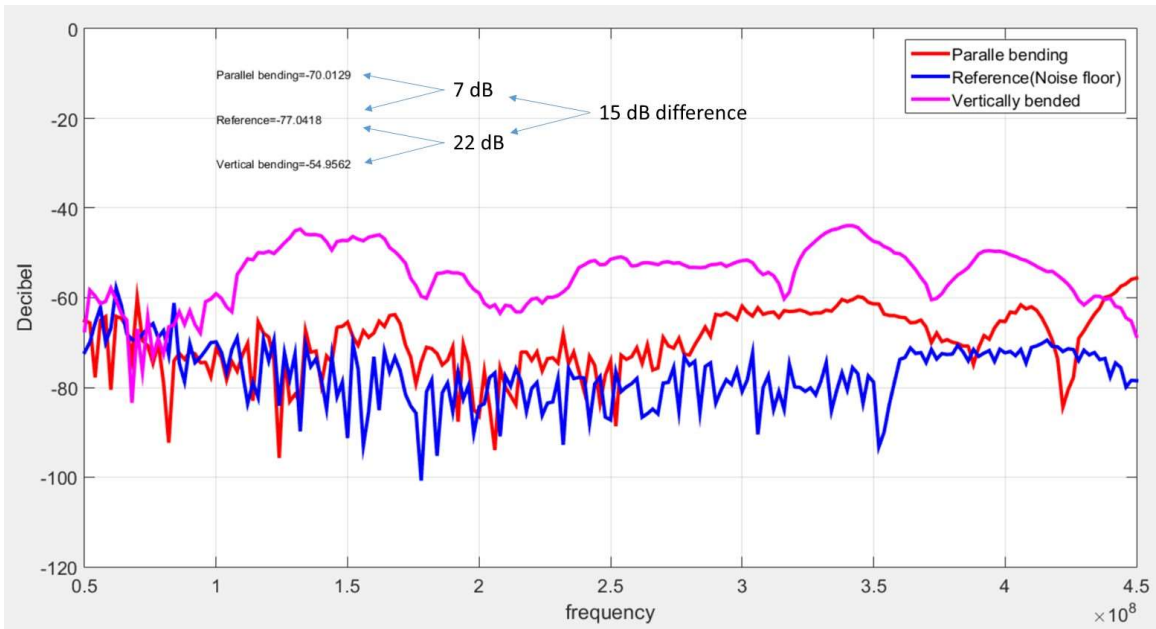


Fig. 3.8. Comparison of the common-mode currents with the vertical bending and with the parallel bending to the copper plane

The antenna-mode current measurements are plotted in Fig. 3.8. As expected, the ratio of common-mode currents is around 15 dB. Although there are some fluctuations due to the resonances of the antenna structure affecting the input impedance at the two source locations, the results show that the calculation of the average increase in the antenna-mode currents is consistent with the change in the imbalance factor.



Fig. 3.9. Test set-up for the detached twin wire pair from the ground wire

Although the harness lost proximity to the ground plane, the twisted pair was always in close proximity to the ground wire. A second test was conducted to examine the consequences of losing proximity to all ground conductors. This test setup is shown in Fig. 3.9. In this setup, the ground wire stays on the ground plane even when the twisted wire pair is routed away from the plane. This situation is a common occurrence in automobiles, because the signals carried on twisted wire pairs are generally considered to be independent of ground.

The antenna-mode currents are measured at the same location and the load is terminated by the same load as the previous setup. In this case, the strength of the two mode conversion sources is higher, because the change in the imbalance factor is higher. The value of h_{\perp} for the harness with a ground wire 45 cm above the plane was 0.3863. Without the ground wire, the value for h_{\perp} is approximately 1. Repeating the calculations in (3.3) with the new value for h_{\perp} yields,

$$\begin{aligned}
 h_{\parallel} &= 0.0305 \\
 h_{\perp} &\approx 1 \\
 V_{AM\perp} &= (h_{\perp} - h_{\parallel})V_{CM} = 0.97V_{CM} \quad \leftarrow \text{first source} \\
 V_{AM2\perp} &= \frac{5.44 \text{ mA}}{8.72 \text{ mA}} V_{AM\perp} = 0.60V_{CM} \quad \leftarrow \text{both sources}
 \end{aligned} \tag{3.5}$$

Note that the antenna-mode voltage, $V_{AM2\perp}$ is $20 \log \left(\frac{0.60 V_{CM}}{0.222 V_{CM}} \right) = 8.7$ dB stronger when the ground wire does not stay with the twisted wire pair. Therefore, the magnitude of the antenna-mode current for the configuration where the twisted wire pair loses proximity to the ground wire should be about 8 – 10 dB higher than the magnitude of the current on the harness that loses proximity to the plane, but maintains proximity to the ground wire.

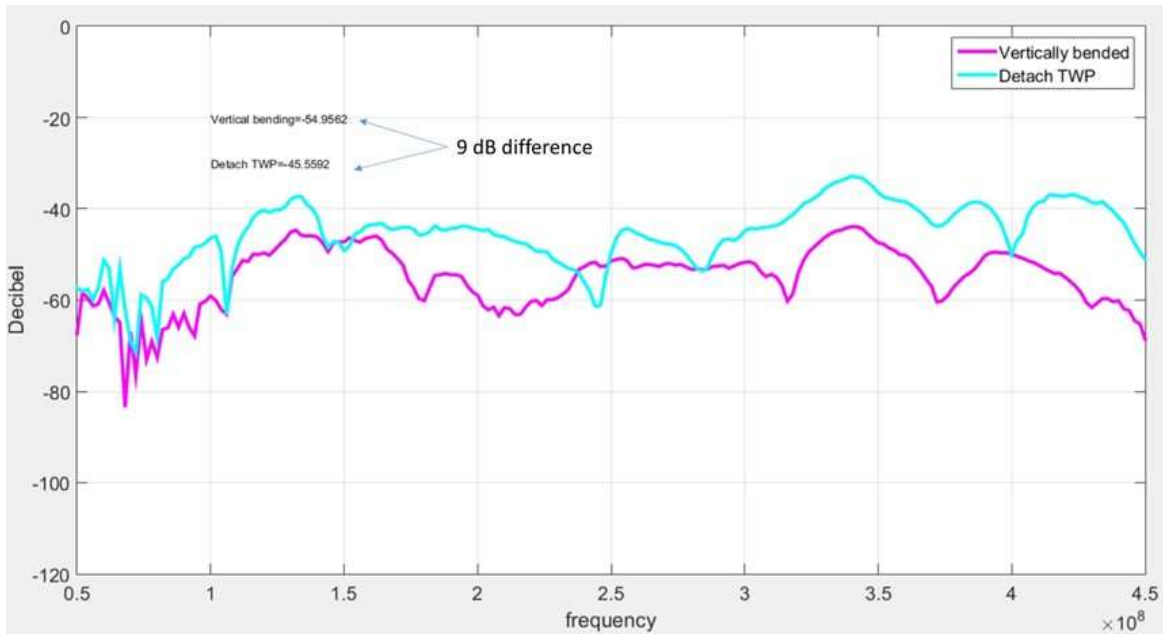


Fig. 3.10. Effect of losing the ground wire from the signal wires

The measured results are plotted in Fig. 3.10. The pink line is the antenna-mode current measured when the ground wire is routed with the twisted wire pair. The cyan line is the antenna-mode current when the TWP loses proximity to the ground wire. As expected, the average difference of the common-mode currents is approximately 9 dB.

3.4 Conclusion

In this paper, the effect of ground proximity on antenna-mode currents induced in wire harnesses was studied. Conversion to antenna-mode currents occurs when there is a change in the electrical balance. Automotive wire harnesses experience changes in the imbalance factor depending on the distance from the wire harness to the ground structure. Even when a ground wire is routed along with a CAN bus wire pair, significant antenna-mode currents are created when the proximity to the ground structure changes. The

antenna-mode currents can be estimated using the imbalance difference method based on changes in the electrical balance of the structure.

References

- [1] C. R. Paul, *Introduction to Electromagnetic Compatibility*, vol. 184. John Wiley & Sons, 2006.
- [2] T. Watanabe, O. Wada, T. Miyashita, and R. Koga, "Common-mode-current generation caused by difference of unbalance of transmission lines on a printed circuit board with narrow ground pattern," *IEICE Trans. Commun.*, vol. 83, no. 3, pp. 593–599, 2000.
- [3] T. Watanabe, H. Fujihara, O. Wada, R. Koga, and Y. Kami, "A prediction method of common-mode excitation on a printed circuit board having a signal trace near the ground edge," *IEICE Trans. Commun.*, vol. 87, no. 8, pp. 2327–2334, 2004.
- [4] L. Niu and T. H. Hubing, "Rigorous Derivation of Imbalance Difference Theory for Modeling Radiated Emission Problems," *IEEE Trans. Electromagn. Compat.*, vol. 57, no. 5, pp. 1021–1026, 2015.
- [5] C. R. Paul, "Effect of Interspersed Grounds on Radiated Emissions", in *Handbook of Electromagnetic Compatibility*. Academic Press, pp985–987, 2013.
- [6] C. Su and T. H. Hubing, "Calculating Radiated Emissions Due to I / O Line Coupling on Printed Circuit Boards Using the Imbalance Difference Method," vol. 54, no. 1, pp. 212–217, 2012.
- [7] H. Kwak and T. H. Hubing, "Investigation of the imbalance difference model and its application to various circuit board and cable geometries," in *Electromagnetic Compatibility (EMC), 2012 IEEE International Symposium on*, 2012, pp. 273–278.
- [8] Y. Toyota, K. Iokibe, and L. R. Koga, "Mode conversion caused by discontinuity in transmission line: From viewpoint of imbalance factor and modal characteristic impedance," *EDAPS 2013 - 2013 IEEE Electr. Des. Adv. Packag. Syst. Symp.*, pp. 52–55, 2013.
- [9] T. Hubing and L. Niu, "Application of the Imbalance Difference Method to the EMC Design of Automotive ECUs," in *Electromagnetic Compatibility, Tokyo (EMC'14/Tokyo), 2014 International Symposium on*, pp. 453–456, 2014.
- [10] Y. Toyota, S. Kan, and K. Iokibe, "Modal Equivalent Circuit of Bend Discontinuity in Differential Transmission Lines," in *Electromagnetic Compatibility, Tokyo (EMC'14/Tokyo), 2014 International Symposium on*, vol. 1, no. c, pp. 117–120, 2014.
- [11] H. W. Shim and T. H. Hubing, "Model for estimating radiated emissions from a printed circuit board with attached cables due to voltage-driven sources," *IEEE*

Trans. Electromagn. Compat., vol. 47, no. 4, pp. 899–907, 2005.

- [12] Y. Toyota, T. Matsushima, K. Iokibe, R. Koga, and T. Watanabe, “Experimental validation of imbalance difference model to estimate common-mode excitation in PCBs,” *2008 IEEE Int. Symp. Electromagn. Compat.*, pp. 1–6, 2008.
- [13] R. K. Tetsushi Watanabe, Hiroshi Fujihara, Osami Wadaz, Akihiro Namba, Yoshitaka Toyotazn, “High-speed Common-Mode Prediction Method for PCBs Having a Signal Line Close to the Ground Edge,” *IEEE Int. Symp. Electromagn. Compat.*, vol. 1, no. 2, pp. 28–33, 2003.
- [14] T. Watanabe, O. Wada, Y. Toyota, and R. Koga, “Estimation of common-mode EMI caused by a signal line in the vicinity of ground edge on a PCB,” *IEEE Int. Symp. Electromagn. Compat.*, vol. 1, pp. 113–118, 2002.
- [15] J. Ahn and T. H. Hubing, “Evaluation of the Common Mode Voltage Generated by Different CAN Transceivers,” *Clemson Veh. Electron. Lab. Technical Rep. CVEL-18-068*, 2018.
- [16] J. Ahn and T. H. Hubing, “Application of Imbalance Difference Method to the EMC Design of Automotive Wire Harnesses,” *Clemson Veh. Electron. Lab. Technical Rep. CVEL-18-072*, 2018.